The *Stenotrophomonas maltophilia* MntR miniregulon includes novel extracytoplasmic components and affects replication in *Acanthamoeba castellanii* phagosomes

Fulvia-Stefany Argueta-Zepeda[1,2], Javier Rivera[1], Julio César Valerdi-Negreros[1,3] https://orcid.org/0000-0001-7536-5483, Christopher Rensing[4] https://orcid.org/0000-0002-5012-7953, and Pablo Vinuesa[1] https://orcid.org/0000-0001-6119-2956

[1]Centro de Ciencias Genómicas, Universidad Nacional Autónoma de México (UNAM), Cuernavaca, Morelos, México

[2]Programa de Maestría y Doctorado en Ciencias Bioquímicas, UNAM, Mexico City, Mexico

[3]Programa de Doctorado en Ciencias Biomédicas, UNAM, Mexico City, Mexico

[4]Fujian Agriculture and Forestry University, Fuzhou, China.

Address correspondence to Pablo Vinuesa, vinuesa@ccg.unam.mx

Keywords: metal-homeostasis, transcriptomics, host-microbe interactions, intracellular replication, nutritional immunity, free-living amoebae, oxidative stress

ABSTRACT

Manganese homeostasis is crucial for opportunistic pathogens such as *Stenotrophomonas maltophilia,* which switch lifestyles between contrasting environments. This study elucidated the manganese homeostasis system in *S. maltophilia* strain Sm18, a Mexican environmental isolate, revealing a sophisticated network that includes conserved and novel components. We focused on the MntR miniregulon, which comprises the well-known inner membrane importer MntH and exporter MntP, both regulated by the Mn^{2+}-responsive MntR metalloregulator. However, it also contains a TonB-dependent receptor (TBDR) with a distinctive CQNC motif likely involved in Mn^{2+} coordination and a periplasmic thioredoxin-fold protein (pTFP). Both are co-expressed from a bicistronic operon under severe manganese and iron limitations and belong to novel families with a limited phyletic distribution. Transcriptomic profiling under varying Mn and Fe concentrations revealed a tight interplay between these metals, emphasizing the ferrophilic nature of *S. maltophilia* and the differential expression of MntR regulon core members. Additional transporters of the RND and CDF families were modulated under dual metal limitation. Mutant analysis demonstrated that MntP is critical for survival, even at Mn levels that do not affect growth kinetics. MntH is required for optimal growth under oxidative stress and intracellular replication within *Acanthamoeba castellanii* phagosomes, highlighting its role in overcoming nutritional immunity. Our findings provide new insights into the remarkable adaptability of *S. maltophilia* to diverse environments, contributing to its success as an opportunistic pathogen causing a broad range of infections in humans.

1. Introduction

Stenotrophomonas maltophilia is a gram-negative, non-fermentative bacterium recognized for its ecological versatility and opportunistic pathogenicity (Brooke, 2021). It thrives in diverse environments, including soil, water, plant rhizospheres, free-living amoebae, and diverse animal organs and cells, demonstrating remarkable adaptability to contrasting ecological niches (Ochoa-Sánchez and Vinuesa, 2017; Rivera et al., 2024; Ryan et al., 2009). These bacteria can survive harsh conditions, such as oligotrophic or metal-rich environments, and are highly resistant to disinfectants and multiple drugs due to robust biofilm formation and multiple efflux systems. Recent research has highlighted these adaptive mechanisms, showing how they enhance the resilience and persistence of *S. maltophilia* in nosocomial environments (Brooke, 2021, 2012), making it one of the ten most prevalent microorganisms in hospital care units

(Rello et al., 2019). This pathogen primarily affects immunocompromised individuals, leading to respiratory tract, bloodstream, and urinary tract infections (Brooke, 2021), and poses a significant challenge in clinical settings because of its intrinsic resistance to multiple antibiotics, including carbapenems (Chang et al., 2015; Ochoa-Sánchez and Vinuesa, 2017). However, little is known about the genes and mechanisms involved in the adaptation of *Stenotrophomonas* to host-associated and intracellular lifestyles in diverse host tissues and phagocytic cells, including free-living amoebae (Denet et al., 2018; Rivera et al., 2024) and mammalian macrophages (Takahashi et al., 2020). In recent years, mounting evidence has revealed that professional phagocytes subject ingested bacteria to limiting or toxic concentrations of transition metals, inhibiting their proliferation in phagosomes, a process known as nutritional immunity (Murdoch and Skaar, 2022).

Homeostasis of essential transition metals, such as manganese, iron, copper, and zinc, is crucial for various physiological processes (Palmer and Skaar, 2016; Waldron and Robinson, 2009). Metallostasis is maintained by a network of allosteric metalloregulators, metal transporters, metallochaperones, and efflux pumps (Porcheron et al., 2013). The concerted action of these components regulates the intracellular metal concentrations, ensuring that they are available for essential functions without reaching toxic levels (Chandrangsu et al., 2017). The ability of bacteria to rapidly adapt to different environments is tightly coupled to their metal homeostasis capabilities, particularly during host infection, as metal concentrations vary widely across organs, tissues, and cellular compartments (Kehl-Fie et al., 2013; Pompilio et al., 2014).

Studies on *S. maltophilia* metallostasis have focused on iron homeostasis, highlighting its importance in bacterial virulence (Mikhailovich et al., 2024). In contrast, our knowledge of the molecular mechanisms underlying manganese homeostasis in *Stenotrophomonas* is limited to a single transcriptomic study performed on *Stenotrophomonas* sp. MNB17, an organism isolated from a deep-sea mud sample in the western Pacific, removes Mn^{2+} by efficiently forming Mn-precipitates ($MnCO_3$ and Mn oxides) at high Mn concentrations (Song et al., 2022). However, manganese homeostasis has been well studied in some Gram-positive and Gram-negative bacteria (Bosma et al., 2021; Waters, 2020). A crucial component is the manganese transporter protein MntH, which facilitates manganese uptake into the cytoplasm under limiting conditions (Kehres et al., 2000). Conversely, the conserved MntP exporter removes excess manganese, thereby maintaining intracellular levels within the optimal range (Waters et al., 2011). This process is regulated by various regulatory proteins and signaling pathways that sense intracellular manganese levels and adjust the expression or activity of

manganese transporters (Bosma et al., 2021; Martin and Waters, 2022; Sengupta et al., 2018; Wright et al., 2024), with MntR being the master regulator (Que and Helmann, 2000; Waters et al., 2011). Furthermore, under manganese limitation and oxidative stress, a Mn^{2+}-scavenging pathway has been identified in *Burkholderia thailandensis*, comprising a newly discovered TonB-dependent outer membrane (OM) manganese transporter, MnoT, and a Mn^{2+}-binding protein, TseM, secreted by a type VI secretion pathway (T6SS) which is apparently unique to Burkholderia species (Si et al., 2017). The requirement for Mn^{2+} and Fe^{2+} varies greatly among bacterial species (Bosma et al., 2021). *S. maltophilia* features an iron-centric metabolism that requires iron for optimal growth and virulence (Kalidasan et al., 2018; Mikhailovich et al., 2024). However, Mn^{2+} becomes essential under oxidative stress or low iron availability (Anjem et al., 2009), conditions that mirror the environments that *S. maltophilia* likely encounters as an intracellular opportunistic pathogen in phagosomes subjected to nutritional immunity (Čapek and Večerek, 2023; Murdoch and Skaar, 2022). This bacterium has been reported to survive in human epidermoid epithelial cells (Zhang et al., 2024), human lung epithelial cells (DuMont et al., 2015; Nas et al., 2019), free-living amoebae (Denet et al., 2018; Rivera et al., 2024), and mammalian macrophages (Nas et al., 2019; Takahashi et al., 2020). The divalent Mn^{2+}/Fe^{2+} transporter Nramp1 protein, located in the phagosomal membrane and ubiquitous in eukaryotes, plays a crucial role in nutritional immunity by depleting phagocytosed bacteria of these micronutrients. Interestingly, its bacterial homolog, MntH, is also essential for countering this stress by importing Mn^{2+} into bacterial cells (Cellier, 2001; Juttukonda and Skaar, 2015).

Here, we present a detailed phylogenomic and functional analysis of *Stenotrophomonas* manganese homeostasis systems, demonstrating their contribution to bacterial fitness in *Acanthamoeba castellanii* phagosomes for the first time. We identified the key components of the MntR miniregulon in *S. maltophilia* Sm18, a Mexican environmental isolate with complete genome sequence (Ochoa-Sánchez and Vinuesa, 2017; Vinuesa et al., 2026), and subjected them to genetic and functional analyses. We demonstrated that the Sm18Δ*mntP* deletion strain was susceptible to Mn^{2+} *in vitro*. We identified two novel genes as members of the miniregulon. They are organized in an operon, encoding a TonB-dependent receptor (TBDR) featuring a conserved CQNC motif, and a periplasmic thioredoxin-fold protein (pTFP), and have not been previously reported to be manganese-regulated. Phylogenomic and comparative genomic analyses revealed that both proteins belong to novel families. RNA-Seq-based transcriptome analyses performed under limiting iron and manganese concentrations revealed that the TBDR-pTFP locus and *mntH* gene are derepressed,

underscoring their importance in maintaining metal homeostasis in metal-restricted environments such as the phagosomes of diverse phagocytes. We recently reported that Sm18 can survive and replicate in the acidified Rab7A-positive vacuoles of *Acanthamoeba castellanii* trophozoites (Rivera et al., 2024). Here, we show that the *mntH* gene is expressed and required for optimal intracellular replication in the phagosomes of this free-living professional phagocyte.

2. Material and methods

2.1 Bacterial strains and culture conditions

Stenotrophomonas maltophilia ESTM1D_MKCAZ16_6a (Sm18) was isolated from the sediments of a clean river in Morelos, Mexico (Ochoa-Sánchez and Vinuesa, 2017), and has its complete genome sequenced (Vinuesa et al., 2026). Sm18 was routinely cultivated aerobically in Lysogeny Broth (LB) at 30°C or in MOPS, previously proven effective for cultivating *Pseudomonas* strains, using 0.4 % (w/v) glucose as the carbon source (LaBauve and Wargo, 2012). We optimized minimal medium MOPS (MM) for *S. maltophilia* growth by adding thiamine and biotin at 0.5% and 0.1% (w/v), respectively, along with 0.2% (w/v) Bacto™ casamino acids (CAA). Our MM lacks manganese in the micronutrient stock. For the growth kinetics, LB was supplemented with 10mM of MOPS buffer (pH 6.8) and antibiotics, as required.

2.2 Generation of markerless deletion mutants

Two genomic DNA fragments flanking the *mntP* gene were PCR-amplified using total DNA from Sm18 as the template with primer pairs Sm18DmntP_PCR1.FOR/ Sm18DmntP_PCR1.REV (570 bp) and Sm18DmntP_PCR2.FOR / Sm18DmntP_PCR2.REV (512 pb). The amplicons were cloned in pEX18Tc (Hoang et al., 1998) linearized with EcoRI and HindIII using NEBuilder HiFi DNA Assembly Master Mix (New England Biolabs, NEB), following the manufacturer's instructions, and transformed into chemically competent *E. coli* DH5α. The resulting suicide vector pEX18Tc::DmntP was transferred into Sm18 by conjugation from *E. coli* S17-1, selecting for Sm18 merodiploids on LB plates supplemented with 20 µg/mL tetracycline and 30 µg/mL gentamicin. Sm18 merodiploids were grown in LB without NaCl and supplemented with 10% sucrose directly from glycerol stocks to select for double recombinants. Markerless deletion mutants were confirmed by tetracycline sensitivity,

colony PCR, and amplicon sequencing (primers Sm18DmntP_VER.F/Sm18DmntP_VER.R; Supplementary Tables A4, A5, and A6). The same procedure was used to generate markerless deletions of *orf02357*, *orf02358*, and *mntH*.

2.3 Generation of Vector Integration Mutants (VIM)

An internal (401 bp) DNA fragment from the coding region of the *mntP* gene in Sm18 was PCR amplified using primers Sm18-VIM-*mntP*.F1/Sm18-VIM-*mntP*.R1 (Supplementary Tables A4, A5, and A6), directionally cloned into the *Ba*mHI and *Hin*dIII sites of pEX18TcVIM-GFP, and transformed into chemically competent *E. coli* DH5α following standard procedures. pEX18TcVIM-GFP_D*mntP* was transferred to Sm18 by conjugation from *E. coli* S17-1. The same procedure was used to generate VIM derivatives of *orf02357* and *mntH*.

2.4 Construction of Sm18 expression plasmids

We modified standard SEVA plasmids (Martínez-García et al., 2023) for the construction of pSEVA327 (oriVRK2, Cm^R) and pSEVA337R (oriVpBBR1, Cm^R) bacterial expression plasmids, following the standardized SEVA modular architecture and nomenclature. Intergenic regions of *orf02357*, *mntH,* and *mntP* were amplified by PCR from genomic DNA using Phusion polymerase (NEB) and primers listed in Supplementary Tables A4, A5 and A6. Selected vectors and amplicons were digested with proper restriction enzymes and directionally cloned upstream of the promoterless reporter genes (GFP or mCherry) to generate the Sm18 expression plasmids 327-*02357_02358*, 327-*mntH*, 327-*mntP*, 337R-*02357_02358*, 337R-*mntH,* and 337R-*mntP* (Supplementary Tables A4, A5 and A6).

2.5 Fluorescence kinetics and microbial growth

The Fluorescence and growth kinetics of strains carrying transcriptional fusions were assessed across three or more biological replicates in 96-well microplates. The bacterial optical density (OD_{600}) was adjusted to 0.05 in LB and 0.01 in MM at a final volume of 200 µL of medium supplemented with increasing $MnCl_2$ concentrations. For growth kinetics, cultures were grown at 30°C and 205 rpm in a Biotek Epoch 2 microplate spectrophotometer, with OD_{600} readings taken every 30 or 45 min. The same setup was used for fluorescence kinetics analysis, with fluorescence (GFP: 479/ 520 nm) and growth (600 nm) measurements recorded in parallel using a BioTek Synergy H1 microplate reader.

2.6 Statistical analysis of fluorescence and growth kinetics

Uninoculated wells with LB or MM served as blanks for microbial growth curves, while strains carrying empty plasmids served as controls. Fluorescence measurements were normalized with OD_{600} readings. The non-parametric Kruskal-Wallis test was used to compare the medians across independent groups based on the Area Under the Curve (AUC) calculated using the Growthcurver R package (v. 0.3.1). When significant differences were detected, Dunn's *post hoc* pairwise comparisons were performed, applying the Bonferroni or Benjamini-Hochberg (BH) correction for multiple testing, as appropriate. Bootstrapping of AUC data was used to compute 95% confidence intervals (CI), represented as error bars in the corresponding figures. All statistical analyses and graphs were performed in R (v 4.3.2), using the ggplot2 (v 3.5.1), ggpubr (v 4.3.2) and rstatix (v0.7.2) packages. Error bars on the growth kinetic graphs represent the standard error of the mean for the technical and biological replicates.

2.7 Cell sample preparation for RNA-sequencing

Three biological replicates were obtained from glycerol stocks stored at -80°C and cultured on LB agar at 30°C for 34 h to isolate colonies with a one-day interval between each replicate. A single isolated colony was subcultured in 3 mL of MM and incubated at 30°C with agitation at 205 rpm for 24 h. Precultures (1:50 dilution) were established in 25 mL of MM in a 50 ml Erlenmeyer flask and incubated at 30°C/205 rpm for 14 h. 10 mL of the pre-cultures were collected by centrifugation (5000 × g for 5 min), washed three times with 5 mL of MM without Fe (MM-Fe0), resuspended in 5 mL of the same culture medium, and used to inoculate four 25 ml flasks with metal-supplemented MM media at OD_{600} ~ 0.005, labeled as MM-Fe0Mn0, MM-Fe0Mn8, MM-Fe10Mn0, and MM-Fe10Mn8. For all conditions, Sm18 cultures were incubated at 30 °C/205 rpm until reaching the early log phase (OD_{600} 0.1-0.2), after which the cultures were split into two technical replicates, and the cells harvested by centrifugation. Immediately, the pellets were covered with 900µL of RNA later. One technical replicate was stored at 4°C until shipped to GENEWIZ from Azenta Life Science for library preparation and sequencing. The other was stored at -80°C for subsequent experiments. Standard RNA-seq (150 bp paired-end reads) was performed on an Illumina HiSeq 2500 platform.

2.8 RNA-seq analysis data and gene expression

Read quality assessment was performed using Fastqc v 0.12.1 (Andrews, S., 2010), using Trimmomatic v 0.39 (Bolger et al., 2014) to trim the index adapter and the initial 15 bp from each read, resulting in 135 bp reads and > 23 million paired-end reads per sample. The complete genome sequence of S. maltophilia strain ESTM1D_MKCAZ16_6a ((Vinuesa et al., 2026); CP146374) served as the reference for aligning the reads using Bowtie2 v 2.4.4 (Langmead and Salzberg, 2012). SAM files generated by Bowtie2 (overall alignment rate per sample >96%) served as input for featuresCounts from the R-Bioconductor software package Rsubreads v 2.14.2 (Liao et al., 2019). FeaturesCount generated an expression matrix containing the expression values of each sample for every gene using the GFF genome annotation file (successfully assigned alignments per sample >92%). Differential gene expression analysis between treatments was performed using the DESeq2 v1.42.0 (Love et al., 2014) package, which normalizes the raw counts through the median of ratios method and conducts differential expression analysis based on the negative binomial distribution of the data. DESeq2 adjusted p-values using Benjamini and Hochberg's method were used to reduce the false discovery rate. Differentially expressed genes (DEGs) were identified using the adjusted p-value (Padj) < 0.01 and log2 fold change ≥ 1 or ≤ -1 as cutoffs. The protein sequences of DEGs were analyzed using the UniProt database (The UniProt Consortium, 2017), InterProScan (Blum et al., 2025), and MOTIF search (https://www.genome.jp/tools/motif/) to assign functions and Gene Ontology (GO) terms.

2.9 Identification of transcription factor binding sites and protein homologs

We used the motif discovery algorithm MEME (v 5.5.5) from the MEME suite (Bailey et al., 2015) to identify 16 to 25 nt long sequence motifs in the 5'-UTR regions of *Stenotrophomonas mntH* (V8P27_002360) orthologs identified with GET_HOMOLOGUES (Contreras-Moreira and Vinuesa, 2013). The resulting position-specific probability matrices (PSPMs) were compared with entries in the CollecTF (Erill, 2015) and PRODORIC (Dudek and Jahn, 2022) databases of experimentally validated transcription factor-binding sites in bacteria, using TOMTOM (v 5.5.5) to determine the identity of the discovered motifs. The collection of 5'-UTR regions containing the MntR-box motif was extended by adding new hits discovered by MAST (v 5.5.5) scans of complete genome sequences representative of the currently described taxonomic diversity of *Stenotrophomonas* and related genera in the *Lysobacteriaceae* (Chauviat et al., 2025; Vinuesa et al., 2018). Homologs of the *S. maltophilia* MntR miniregulon proteins were identified by hmmsearch (v3.4) from the HMMER3 suite (44)

using the gathering threshold (--cut_ga) option for calibrated profile hidden Markov models (HMMs) retrieved from Pfam (PF01566 for MntH, PF02659 for MntP), or built locally with hmmbuild (v3.4) from clustal omega (Sievers and Higgins, 2018) alignments (with –iter 2 and –use-kimura options) of our curated datasets of MntR, V8P27_002357, and V8P27_002358 homologs. The latter three HMMs and the PSPM for the *Lisobacteraceae* MntR-box are available for download from https://github.com/vinuesa/supplementary_materials/.

2.10 Live-cell imaging (LCI) using widefield fluorescence microscopy of Sm18/337R-mntH in co-culture with A. castellanii

The assay was reported in detail by (Rivera et al., 2024). Briefly, co-cultures were established by seeding 20-mm diameter glass-bottom cell culture dishes with 5×10^5 *A. castellanii* strain Neff trophozoites, which were incubated for 1 h at 30°C in MMsalts-MOPS-Glc medium. *S. maltophilia* Sm18/337R-*mntH* was grown in LB, washed, and adjusted to an OD_{600} of ~1.0 (~4.8×10^8 CFU/mL). Diluted bacterial suspensions were added to the culture dishes to achieve a multiplicity of infection (MOI) of 25, followed by centrifugation at 500 × g for 5 min to synchronize phagocytosis. LCI was performed using an AxioVertA1 inverted microscope (Karl Zeiss) at three and 18 h ppc.

2.11 Quantitative evaluation of the intracellular replication of mutant strains Sm18VIMmntH and Sm18ΔmntR in Acanthamoeba trophozoites

Experiments were performed using the microtiter plate assay described by (Rivera et al., 2024). Briefly, each well contained 1×10^5 trophozoites in MMsalts-MOPS-Glc and was incubated for 30 min at 25°C. After replacing the medium with the tagged bacteria (Sm18VIM*mntH*::mTn7_Pc_mScarlet-I and Sm18Δ*mntR*::mTn7_Pc_mScarlet-I mutants) at MOI10, phagocytosis was synchronized by centrifugation at 500 × g for 5 min, and the plates placed in a plate reader Synergy 2 and incubated statically at 25°C. Red fluorescence was measured every 30 min for 48 h at 568 nm/594 nm (excitation/emission). The controls included wells with medium, trophozoites in the medium, or bacteria in the medium.

3 RESULTS

3.1 Manganese tolerance of S. maltophilia Sm18 in complex and defined media

To assess the strain's manganese tolerance, we ran 48-hour growth kinetics using complex lysogeny broth (LB) and minimal MOPS (MM) media with increasing $MnCl_2$ concentrations. Fig. 1A shows that Sm18 grew in LB and MM up to 16 mM and 8 mM of $MnCl_2$, respectively. In both media, the maximal growth rate and total yield of the culture remained unaffected, except at the highest Mn concentration tested. However, statistical analysis of the area under the curve (AUC) for population density (OD_{600}) data (Fig. 1B) revealed a significant decrease in growth in both media starting at 8 mM $MnCl_2$, due to the extended lag phase observed with increasing Mn concentrations. These results indicate that Sm18 exhibits notably higher tolerance to manganese than other gram-negative bacteria, such as *Escherichia coli (Zeinert et al., 2018)*.

3.2 Genome-wide identification of manganese-responsive genes in S. maltophilia Sm18 by RNA-seq analysis under varying manganese and iron concentrations

To identify Sm18 genes involved in Mn^{2+} hemostasis under contrasting Fe^{2+} regimes, we analyzed the transcriptional profile of Sm18 cultures (three biological replicates per treatment) using RNA-sequencing (RNA-Seq). Cultures were established in defined MM medium supplemented with casamino acids, under four combinations of Fe^{2+} and Mn^{2+} in micromolar (μM) concentrations: (i) Fe0 Mn0, (ii) Fe0 Mn8, (iii) Fe10 Mn0, and (iv) Fe10 Mn8. Principal component analysis (PCA) shown in Fig. 2A demonstrated that replicates within each group were clustered and separated according to metal concentration. PC1 revealed that 64% of the variance was related to varying iron conditions, while PC2 explained 10% of the variance due to manganese concentrations, supporting the classification of Sm18 as a bacterium with an iron-centric metabolism. To validate this hypothesis, we conducted differential gene expression analysis using DESeq2. We identified a total of 124 DEGs when comparing Fe^{2+} 10 μM vs. Fe^{2+} 0 μM in MM-Mn0, and 89 DEG in MM-Mn8, based on an adjusted *p*-value (padj) < 0.01 and a $\log_2$ fold change $|(\log_2 FC)| \geq 1.0$ (see Methods). In contrast, only five DEGs were detected when comparing Mn^{2+} 0 μM vs. Mn^{2+} 8 μM in MM-Fe10, and 16 DEG in MM-Fe0. The number of DEGs for each condition is summarized as a Venn diagram (Fig. 2B), revealing that 88 DEGs were regulated solely by iron levels, irrespective of manganese concentrations in the medium. A detailed analysis of these genes will be presented elsewhere (Argueta-Zepeda and Vinuesa, *in preparation*). Among the elements of the MntR miniregulon

310 in Sm18, *mntP* is the only gene exclusively regulated by manganese levels in the medium,
311 independent of iron availability (Fig. 2B). In contrast, the expression of *mntH* was affected by
312 any change in Mn or Fe concentration (Fig. 2B). The latter result aligns with previous reports
313 showing that *mntH* transcription is regulated by MntR and Fur (Bosma et al., 2021). Nine
314 genes displayed differential expression only when cultures were subjected to simultaneous
315 Fe^{2+} and Mn^{2+} limitation (Fig. 2B). Two were down-regulated (blue-colored locus tags) under
316 these conditions, whereas the remaining genes were up-regulated, as detailed below. Figure
317 2C highlights the DEGs identified when comparing Mn^{2+} 0 μM vs. Mn^{2+} 8 μM in both MM-Fe10
318 and MM-Fe0 media (see Supplementary Data, Tables A1 and A2 for more details). These
319 DEGs are represented as colored dots on the log_2FC plots, and their corresponding genomic
320 loci are indicated by green vertical bars mapped to the Sm18 chromosome. Their gene
321 ontologies (GOs) are highlighted in different colors with the transmembrane transport
322 category (yellow points) being the most prevalent. Fig. 2C also shows the log_2FC values in a
323 bar plot for a better quantitative representation, including the protein annotations of each
324 DEG. It shows that V8P27_002357, V8P27_002358, and V8P27_004008, encoding a TonB-
325 dependent receptor (TBDR), a periplasmic thioredoxin-fold protein (pTFP), and the well-
326 known cytoplasmic membrane Mn exporter MntP, respectively, display the most significant
327 log_2FC changes, exceeding 2.8 units in absolute values. TBDR and pTFP are circled and,
328 with a few others mentioned below, are likely involved in the Sm18 transition metal
329 homeostasis system under simultaneous manganese and iron limitation. These proteins were
330 subjected to additional bioinformatic, genetic, and functional characterization, as detailed in
331 the following sections. Finally, in MM supplemented with 8 μM Mn^{2+}, *mntH* expression was
332 repressed, whereas *mntP* showed a >3 Log_2FC increase, presumably to export excess
333 cytoplasmic manganese. Furthermore, in the absence of Fe supplementation, other genes
334 were up-regulated along with *mntP*, including four predicted transporter proteins (Fig. 2C). In
335 contrast, five genes primarily associated with transmembrane transport were down-regulated
336 together with *mntH*, V8P27_002357, and V8P27_002358 (Fig. 2C).
337

338 *3.3 Genome-wide scanning for potential MntR binding sites identified the core components of*
339 *the MntR mini regulon in S. maltophilia Sm18*

340 Several Mn^{2+}-responsive genes are known to be regulated by MntR, the master allosteric
341 manganese transport metalloregulator of the DtxR family (Patzer and Hantke, 2001), which
342 recognizes a short inverted palindromic sequence in the 5' UTR region of target loci known as

the MntR-box. We performed iterative MEME-MAST (Bailey et al., 2015) searches using 5'-UTR regions of *Stenotrophomonas mntH* (V8P27_002360) orthologues (see Methods) to identify potential MntR-boxes in a collection of 103 Lysobacteraceae genomes described in the following section, resulting in the MEME profile shown in Fig. 3A. MAST-based (Bailey et al., 2015) genome-wide scanning of the Sm18 assembly with the MntR-box profile revealed the presence of two additional MntR boxes, defining two additional genomic loci potentially under MntR regulation. The first site mapped 75 bp upstream of the putative V8P27_002357 (*orf2357*) start codon, which was shown by RNA-seq to be the DEG with the highest $\log_2$FC value of those displaying differential regulation specifically under both Mn^{2+} and Fe^{2+} limitation (Figs. 2B and 2C), and closely linked to the *mntR* (V8P27_002359) and *mntH* genes. The latter two share a bidirectional promoter, with the MntR-box positioned 10 bp upstream of the *mntH* putative start codon (Fig. 3B). The third site maps 247 bp upstream of the putative *mntP* start codon which is differentially expressed in media with high Mn^{2+} concentrations, irrespective of Fe^{2+} concentration. Similar to *E. coli*, *mntP* in Sm18 is preceded by a putative *yybP-ykoY-like* riboswitch (Fig. 3C). Based on this evidence, we postulated that *orf2357, orf2358, mntH* and *mntP* (Fig. 3B and 3C) form the core of a putative MntR miniregulon in *S. maltophilia* Sm18, similar to that defined by (Waters et al., 2011) for *Escherichia coli*. Interestingly, *orf2357* and *orf2358*, are not found in MntR regulons reported in other bacteria (Martin and Waters, 2022).

3.4 Phylogenomic analysis revealed a lineage-specific distribution of MntR miniregulon core members across Lysobacteraceae

We used hmmsearch from the HMMER3 suite (Eddy, 2011) with calibrated profile hidden Markov models (see Methods) to identify MntR, MntH, MntP, ORF2357 (TBDR), and ORF2358 (pTFP) homologs across a collection of 103 RefSeq genomes representative of the currently described taxonomic diversity of *Stenotrophomonas* and related Lysobacteraceae (Chauviat et al., 2025). Genome-wide MAST scans using the MntR-box profile described in the previous section (Fig. 3A) identified 0 to 4 MntR-boxes per genome at a cutoff P-value ≤ $5e^{-8}$, suggesting that not all genomes contain the MntR miniregulon. To study the phylogenetic distribution of its members, we estimated a maximum likelihood species tree for the 103 genomes based on the concatenated supermatrix of 155 top-scoring core genome proteins selected with GET_PHYLOMARKERS (Vinuesa et al., 2018) out of 601 input core gene families computed with GET_HOMOLOGUES (Contreras-Moreira and Vinuesa, 2013). The

resulting tree was used to map taxonomic information and integrate it with the presence-absence patterns of hmmsearch hits and the count data of MAST hits for the MntR motif (Fig. 4). Only *Stenotrophomonas* species, including *S. maltophilia*, encode these five proteins, which correlates with the presence of three MntR boxes. However, *S. pavanii*, *S. beteli*, and *S. hibiscicola* lack TBDR and pTFP proteins and contain only two MntR boxes each. TBDR and pTFP homologs were not detected in the *Allostenotrophomonas*, *Pseudostenotrophomonas*, and *Parastenotrophomonas* proteomes. Only the MntP exporter was conserved across the four genera analyzed (Fig. 4). In conclusion, within the analyzed Lyosobacteraceae*,* the five-member MntR miniregulon was found to be restricted to species in the *S. maltophilia* complex (Chauviat et al., 2025; Vinuesa et al., 2018).

3.5 The expression of S. maltophilia Sm18 MntR regulon core genes is modulated by iron and manganese concentrations

To validate the bioinformatic predictions supporting the existence of an MntR miniregulon in *S. maltophilia* complex genomes (Figs. 3 and 4), we constructed transcriptional fusions of the 5'-UTRs of each of the three core loci of Sm18 to GFP using the broad-host-range plasmid pSEVA327 (Sm18/327-2357_2358, Sm18/327-*mntH*, and Sm18/327-*mntP;* Supplementary Data, Table A4). Fig. 5A presents the corresponding promoter activities measured over 40 h as the AUC values of GFP relative fluorescence units (RFU), normalized to the population density (OD_{600}), in response to varying Mn and Fe concentrations. Expression data for the Sm18/327-2357_2358 fusion (Fig. 5A, first panel) revealed that the operon encoding the novel TBDR and pTFP protein was expressed solely under Mn and Fe limitation (Mn^{2+} 0 μM and Fe^{2+} 0 μM), consistent with the RNA-seq data (Fig. 2). However, no GFP signal was detected in MM containing 80 nM Mn^{2+}, indicating that low Mn^{2+} concentrations abolish their expression. Activity of the Sm18/327-*mntH* fusion (Fig. 5A, second panel) was negatively correlated with increasing Mn^{2+} concentrations in the culture medium. However, low activity was still measurable at 8 μM Mn^{2+}. A significantly higher activity in the Sm18/327-*mntH* expression profile was observed at Fe^{2+} 10 μM vs. 0 μM, except when the medium contained 8 μM Mn^{2+}. These results confirm a strong relationship between Mn and Fe homeostasis in Sm18, specifically in manganese uptake systems, as revealed by our RNA-seq data, and is consistent with observations made in *E. coli* (Taudte et al., 2016; Wang et al., 2023). In line with our RNA-seq results, the expression profile of Sm18/327-*mntP* increased significantly at 8 μM Mn^{2+}, compared to Mn^{2+} 0μM, irrespective of

Fe availability in the medium (Fig. 5A, third panel). As shown in Fig. 1, although the upper Mn^{2+} concentration (8 μM) used for these experiments is orders of magnitude below the threshold tolerated by Sm18, it is high enough to diminish or abolish the expression of importers and activate the MntP exporter.

3.6 The MntR metalloregulator controls the expression of the core components of the Sm18 Mn homeostasis system

To confirm that the promoter activity observed in the transcriptional fusions reported in Fig. 5A is regulated by MntR, the three fusions were transferred into a Sm18Δ*mntR* strain carrying a markerless *mntR* deletion (Supplementary Data, Table A3). Promoter activity in iron-deficient MM with 0 μM and 8 μM manganese was measured as described in the previous section (Fig. 5A). The Sm18Δ*mntR*/327-2357_2358 fusion (Fig. 5B, first panel) revealed a significant increase in expression in the absence of supplemented manganese, suggesting derepression in the absence of the MntR transcription factor. However, adding manganese led to reduced expression, following a similar trend to that observed in the Sm18 wild-type background, suggesting that manganese may also negatively regulate this operon via an alternative MntR-independent mechanism. Similarly, derepression of the 327-*mntH* fusion was observed in the Sm18Δ*mntR* genetic background compared to the wild-type growing in MM without supplemented manganese (Fig. 5B, second panel). However, no statistically significant activity was detected in the Sm18ΔmntR/327-*mntH* fusion upon addition of 8 μM Mn^{2+}. This suggests that manganese-dependent regulation of *mntH* promoter activity is mediated exclusively by MntR. Finally, the *mntP* fusion exhibited manganese-dependent regulation exclusively through MntR, as no expression was detected in the absence of MntR (Fig. 5B), independent of manganese concentration, in line with the RNA-seq data (Fig. 2).

3.7 The V8P27_002357 TonB-dependent receptor belongs to a novel family with a restricted phylogenetic distribution featuring a conserved CQNC motif in its plug domain

After confirming that V8P27_002357 (TBDR) and V8P27_002358 (pTFP) are members of the MntR miniregulon restricted within Lysobacteraceae to some Stenotrophomonas species (Fig. 4), and are subjected to Mn^{2+} regulation (Figs. 2 and 5), we performed a domain, motif, and phylogenomic characterization of these novel proteins. Fig. 6 summarizes the findings for

V8P27_002357. It encodes a 719 aa TonB-dependent receptor with a 28 bp-long N-terminal signal peptide (Fig. 6A), resulting in a mature protein of 76.6 kDa (691 aa) containing an N-terminal plug or core domain (141 aa, 15 kDa) featuring a centrally located CQNC motif, followed by a TBDR β-barrel domain (550 aa, 61.6 kDa). AlphaFold3 (AF3) (Abramson et al., 2024) modeling of V8P27_002357 in the apo and holo conformations strongly suggests (ipTM = 0.84; pTM =0.90; mean pLDDT = 87.08) that a Mn^{2+} cation could be coordinated by two sulfur, one nitrogen, and one oxygen atom arranged in a tetrahedral geometry, contributed by residues C63, C66 from the CQNC motif, and residues E247, and H446 from the β-barrel domain, respectively (Supplementary Figure S1).

We used BlastP to search for V8P27_002357 homologs (excluding *Stenotrophomonas* hits) in the PDB, Swiss-Prot, and RefSeq protein databases. This analysis revealed a restricted and sparse phylogenetic distribution of the closest hits, which belonged to a few genera in the classes Bacteroidia, Flavobacteriia, Holophagae, Opitutia, Alphaproteobacteria, and Gammaproteobacteria. These sequences were subjected to structure-guided multiple-sequence alignment and maximum likelihood phylogeny estimation (see Methods section). Fig. 6B depicts a small summary tree, revealing that the closest V8P27_002357 homologs form a perfectly supported (100% bootstrap support) and tightly clustered lineage of sequences, all of which share the distinct CQNC motif in their plug domain (Fig. 6C: Fig S1). Based on this evidence, we propose that V8P27_002357-like proteins comprise a new family (CQNC) of TBDRs (Fig. 6B).

3.8 V8P27_002358 belongs to a novel family of periplasmic thioredoxin-fold proteins (pTFPs) linked to CQNC-type TBDRs by synteny and co-expression, featuring a WC[AG]PC motif

The presence of a periplasmic thioredoxin-fold protein (pTFP; matching IPR013766) co-expressed with a preceding CQNC-type TBDR (V8P27_002357 in Sm18) has not been previously reported and suggests that both proteins might be functionally related. To challenge this hypothesis, we performed phylogenomic and comparative genomic analyses of this protein. BLAST searching for V8P27_002358 homologs was done as described in the previous section for the TBDR protein, extending the collection of homologues with the recently reported metagenomic dataset of thioredoxin superfamily proteins compiled by Nilewski et al. (Nilewski et al., 2021), and hmmsearch hits found by screening the Reference Proteomes 2025_01 database through the HMMER portal with our pTFP.hmm profile HMM as the query (see Methods), resulting in a collection of 278 proteins. After alignment with

clustal-omega, the resulting matrix was manually curated, generating a final set of 78 closely-related homologs, including plant sequences automatically annotated (TrEMBL) as protein-disulfide reductases. A maximum likelihood phylogeny was estimated from this set, revealing that V8P27_002358 clustered in a highly supported (99% bootstrap support) and distinct clade (Supplementary Fig. S2) with uncharacterized sequences from a few bacterial genera belonging to the orders Lysobacterales (Gammaproteobacteria), Sphingomonadales (Alphaproteobacteria), and Opitutales (Verrucomicrobiota; Opitutia). Synteny analysis of representative bacterial sequences revealed that the V8P27_002358 clade members were located immediately downstream of the CQNC-type TBDR (Fig. 6D), strongly reinforcing the notion that they are functionally related. However, the genes flanking the TBDR-pTFP locus were variable (Fig. 6D).

V8P27_002358 is a 173 aa long protein and features an N-terminal signal peptide of 23 aa. The mature protein contained 159 aa, with a computed mass of 17.64 kDa and a periplasmic location, as predicted by Phobius (p = 0.94) and Psortb (score = 9.84). All pTFPs share a minimal thioredoxin fold (TRX-fold) characterized by an N-terminal βαβ fold separated by an α-helix from the C-terminal ββα fold (Martin, 1995). The highly diversified and ubiquitous superfamily of pTFPs (Anjou et al., 2024; Atkinson and Babbitt, 2009; Nilewski et al., 2021) encodes thiol:disulfide oxidoreductases (TDORs) that contain additional secondary structural elements and loops inserted between the conserved domains of the TRX fold. Figure 6E displays the highly conserved CXXC (C39, C42) motif of thioredoxins and thioredoxin-like proteins found at the beginning of the α1 helix of the TRX fold, as confirmed by our AF3 modeling (Supplementary Figure S3). V8P27_002358 contains an unusual CAPC dipeptide in the presumed catalytic CXXC redox center. Motif analysis around the β1-α1 region of the TRX-fold, including well-characterized pTFPs (SwissProt codes) with contrasting reduction potentials and pK_a values previously analyzed by Mavridou et al. (Mavridou et al., 2014) revealed a considerable diversity in and around the CXXC motif. The pTFPs associated with CQNC-type TBDRs are characterized by a distinctive and lineage-specific Y[FYC]GA[DS]WC[AG]PCH[AE]F[VL]P profile overlapping the CXXC motif (Fig. 6E).

3.9 Mutants of MntR miniregulon members result in hydrogen peroxide and manganese sensitivity

To investigate whether the Sm18 *mntH* and *mntP* homologs encode functional manganese importer and exporter proteins, we constructed the vector integration mutant (VIM)

506 Sm18VIM*mntH* and the markerless deletion mutant Sm18Δ*mntP* (see Methods). The growth
507 kinetics of the Sm18VIM*mntH* mutant indicated that the *mntH* gene is not essential under
508 Fe^{2+}- or Mn^{2+}-limiting conditions in axenic cultures. However, it is required for growth under
509 oxidative stress induced by hydrogen peroxide (H_2O_2), particularly at neutral pH (Fig. 7A).
510 Statistical analysis revealed that the difference in growth was significant only at 500 μM H_2O_2
511 compered with the wild type (Fig. 7B). These results are consistent with other studies, which
512 demonstrated that *mntH* mutants are sensitive to H_2O_2, a phenotype largely attributed to their
513 impaired ability to import manganese into the intracellular space (Anjem et al., 2009).
514 Conversely, it has been well established in diverse bacterial models that manganese exporter
515 proteins are required to counter manganese toxicity (Waters, 2020; Zeinert et al., 2018).
516 Sm18Δ*mntP* was challenged with increasing Mn^{2+} concentrations (5-160 μM; Fig. 7C), with
517 statistically significant sensitivity detectable at 40 μM, and complete growth inhibition
518 observed at 160 μM (Fig. 7D). The wild-type phenotypes of the Sm18VIM-*mntH* and
519 Sm18Δ*mntP* strains were restored by complementing plasmids Sm18VIM-*mntH*/332::*mntH*
520 and Sm18Δ*mntP*/332::*mntP* provided in *trans*, and carrying the *mntH* and *mntP* genes under
521 the control of their native promoters (Fig. 7). These results demonstrate that *mntH* and *mntP*
522 expression is essential for H_2O_2 resistance and manganese detoxification, respectively, and
523 confirm that the uncovered MntR miniregulon is functional. Notably, no growth phenotypes
524 were detected for the markerless V8P27_002357 and V8P27_002358 mutants under all
525 conditions tested.

526

527 *3.10 The mntH gene of S. maltophilia is expressed in A. castellanii phagosomes and is*
528 *required for optimal intracellular replication*

529 We recently found that *S. maltophilia* Sm18 resists digestion by *A. castellanii* strain Neff
530 trophozoites and can replicate in acidified, Rab7A-positive *Stenotrophomonas*-containing
531 vacuoles (SCV) of this free-living professional phagocyte (Rivera et al., 2024). Given that the
532 phagosomes of *Dictyostelium discoideum* and human macrophages subject bacteria to iron
533 and manganese limitation via the NRAMP exporter (Morey et al., 2015; Peracino et al., 2013),
534 we postulated that the Sm18 MntH Mn importer is required to survive in the SCV. To test this
535 hypothesis, we first evaluated the transcriptional fusion of the *mntH* promoter region to
536 mCherry2 by live-cell imaging (LCI) of *A. castellanii* strain Neff co-cultured with
537 Sm18/pSEVA337R_mntH set at MOI25, using wide-field fluorescence microscopy. As shown
538 in Fig. 8A, the fusion was expressed at 3 and 18 h post-primary contact (ppc). This result

strongly suggests that phagocytosed Sm18 cells experience Mn and possibly Fe limitations in the SCV. We used our *A. castellanii-Stenotrophomonas* co-culture assay in 96-well microtiter plates coupled to a fluorescence reader (Rivera et al., 2024) to evaluate the replication capacity of strains Sm18VIM*mntH* and Sm18Δ*mntR* in trophozoites. We tagged Sm18VIM*mntH* and Sm18Δ*mntR* with our pUC18T_mTn7TC1_Pc_mScarlet-I minitransposon, which constitutively expresses the mScarlet-I fluorescent protein from the strong Pc promoter (Rivera et al., 2024), resulting in strains Sm18VIM*mntH*::mTn7_Pc_mScarlet-I and Sm18Δ*mntR*::mTn7_Pc_mScarlet-I, respectively (Supplementary Data, Table A3). Their replication capacity was compared to that of Sm18 tagged with the same transposon (Sm18:: mTn7_Pc_mScarlet-I). As shown in Fig. 8B, the Sm18VIM*mntH* mutant had a significantly reduced replication capacity in Neff trophozoites compared to Sm18, whereas that of Sm18Δ*mntR* was indistinguishable from that of the wild type strain (Figs. 8B and 8C). These findings support the hypothesis that *Acanthamoeba* phagosomes restrict manganese availability to ingested bacteria and demonstrate that MntH is indispensable for optimal intracellular replication.

4. Discussion

This study provides the first insights into the MntR miniregulon and manganese homeostasis of *Stenotrophomonas maltophilia* and related species, revealing similarities to known systems in other bacteria and novel cell envelope components. As expected, the core elements of the *S. maltophilia* MntR system include the inner-membrane importer and exporter proteins MntH and MntP under the control of the MntR allosteric metalloregulator, which are highly conserved throughout evolution (Martin and Waters, 2022; Waters et al., 2011). However, *S. maltophilia* and other *Stenotrophomonas* species also feature a novel bicistronic operon encoding an outer membrane (OM) TonB-dependent receptor (TBDR, V8P17_002357) and a periplasmic thioredoxin-fold protein (pTFP, V8P17_002358). Gram-negative bacteria typically encode multiple TBDRs, many of which have unknown functions (Blanvillain et al., 2007; Schauer et al., 2008). It is well established that in *S. maltophilia,* iron limitation enhances virulence and biofilm formation (García et al., 2015; Kalidasan et al., 2018), and the expression of TBDRs involved in heme (Shin et al., 2024), hemin (Liao et al., 2024; Shih et al., 2022), and ferri-stenobactin (Wu et al., 2022; Yeh et al., 2025) uptake, as well as others involved in competition for secreted pyochelin siderophores in co-cultures with *Pseudomonas aeruginosa* (Pan et al., 2022). In addition to iron acquisition, *S. maltophilia* TBDRs have been implicated

572 in β-lactam (Calvopiña et al., 2020) and keratin monomer uptake (Xue et al., 2024).
573 *Xanthomonas* species, which are close relatives of *Stenotrophomonas*, feature around 70
574 TBDRs, many of which are required for scavenging plant carbohydrates (Blanvillain et al.,
575 2007). At least 14 TonB-dependent iron acquisition and virulence pathways have been
576 extensively studied in *P. aeruginosa (Hubert et al., 2023)*. Other well-known TBDRs, such as
577 BtuB, OprC, FhuA, and FecA, translocate vitamin B12 (cyanocobalamin), copper, ferric
578 hydroxamate, and Fe^{3+} dicitrate, respectively. However, MnoT (Q2SY62_BURTA) from
579 *Burkholderia* is the only TBDR currently known to import Mn (Si et al., 2017). Analysis of the
580 *S. maltophilia* Sm18 genome (Vinuesa et al., 2026) revealed that it encodes 65 putative
581 TBDRs, representing one of the most expanded paralog gene families in this organism (data
582 not shown). Our MEME-MAST analyses (Fig. 3B) revealed that V8P27_002357 is the only
583 TBDR associated with an MntR-binding box in Sm18. This box is located 75 bp upstream of
584 the putative start codon, between the -10 and -35 regions (Fig. 3B), supporting the notion that
585 MntR is a transcriptional repressor of this locus. Transcriptional fusion and transcriptome
586 profiling data revealed that the *orf2357-orf2358* operon was derepressed only under severe
587 manganese and iron restriction, with its expression virtually abolished upon the addition of 80
588 nM manganese. This correlates with observations of other TBDRs, typically expressed only
589 under severely limiting nutritional conditions (Si et al., 2017; Silale and Van Den Berg, 2023),
590 and highlights the interplay of manganese and iron in the unknown regulatory mechanism of
591 the *orf2357-orf2358* locus. However, the Sm18Δ*orf2357* (TBDR) and Sm18Δ*orf2358* deletion
592 mutants did not exhibit a growth phenotype under these metal-restricted conditions, and the
593 Sm18/337R-pr_*2357-2358* transcriptional fusion was not expressed in co-cultures with *A.*
594 *castellanii* trophozoites (data not shown). Phylogenomic analysis of Sm18 TBDRs and a
595 broad collection of well-classified reference proteins from this family revealed that it belongs
596 to a novel clade possibly involved in Mn uptake, which is unrelated to the *Burkholderia* MnoT
597 clade or typical iron-importing TBDRs mentioned above (data not shown). This conclusion is
598 supported by detailed structrual and motif analyses of V8P27_002357 (Fig S1). Its most
599 distinguishing feature is the presence of a CQNC motif located in the center of the plug
600 domain. Based on the bioinformatic and transcriptional evidence gathered, we hypothesized
601 that V8P27_002357 might function as an OM Mn importer, with the CQNC motif likely
602 involved in Mn^{2+} coordination, as strongly suggested by our AlphaFold3 modeling (Fig. S1).
603 The discovery of a periplasmic thioredoxin-fold protein (pTFP; V8P27_002358) as part of the
604 MntR regulon expands the known components of bacterial manganese homeostasis and
605 thiol-disulfide exchange systems. Furthermore, this finding adds a new layer of complexity to

606 our understanding of how bacteria manage metal homeostasis and oxidative stress in the cell
607 envelopes. Synteny, phylogenetic co-occurrence (Fig. 6D), and co-transcription in a
608 bicistronic operon with the preceding CQNC-type TBDR (V8P27_002357) suggest a
609 functional coupling between both proteins. It is well established that most secreted proteins
610 enter the periplasm via the Sec pathway in an unfolded state (Smets et al., 2019). The
611 periplasm of Gram-negative bacteria is an oxidizing compartment in which sulfur-containing
612 amino acids, such as cysteine and methionine, are particularly vulnerable to oxidation by
613 ROS (Collet et al., 2020). Disulfide bond formation in the periplasm of didermic
614 Gammaproteobacteria is catalyzed by DsbA from the canonical DsbAB pathway as the
615 unfolded intermediate transits through the SecYEG channel (Kadokura and Beckwith, 2009;
616 Landeta et al., 2018). DsbA is a highly oxidizing soluble periplasmic oxidoreductase with a
617 canonical thioredoxin fold and CXXC motif, which is also present in *S. maltophilia* Sm18
618 (V8P27_002985, BsbAsm). Therefore, it is likely that the two consecutive cysteines found in
619 CQNC motif othe CQNC-TBDR are oxidized, forming a disulfide bridge by the action of
620 BsbAsm as it transits into the periplasm through the SecYEG channel during export. In this
621 model, the cognate and specialized periplasmic thioredoxin-fold protein V8P27_002358 is
622 required to reduce the disulfide bond in the CQNC motif as the protein folds and integrates
623 into the outer membrane to fulfill its predicted role as a Mn-importing TBDR. Therefore, we
624 postulate that V8P27_002358 might be a specialized disulfide reductase for the CQNC motif
625 in V8P27_002357 featuring a distinct WC[AG]PC motif (Fig. 6 and Fig. S3). This working
626 model for the novel TBDR-pTFP locus opens new avenues for research into bacterial metal
627 acquisition strategies and thiol-disulfide homeostasis in the periplasm.
628 Regarding the conserved and broadly distributed MntR miniregulon components, this study
629 reports the first genetic analysis of *mntH* in *S. maltophilia*. We demonstrate that it encodes its
630 primary manganese importer protein, and is relevant for replication in amoebal phagosomes.
631 There are several lines of evidence to support this conclusion. The *mntH* gene maps
632 downstream of the *mntR* gene. It is regulated by both manganese and iron availability, as
633 shown by our RNA-seq and transcriptional fusion data, and has been observed in *E. coli* and
634 other bacteria (Martin and Waters, 2022). Furthermore, transcriptome analysis suggests that
635 no other manganese inner-membrane transporter is solely regulated by manganese
636 availability in Sm18. Perhaps most significantly, *mntH* is reported herein for the first time to be
637 required for optimal replication of *S. maltophilia* within *A. castellanii*, a professional phagocyte.
638 This finding has broader implications for understanding the pathogenicity of *S. maltophilia*,
639 suggesting that manganese acquisition contributes significantly to bacterial fitness within host

640 cells. We observed active expression of the *mntH* promoter probe *in vivo* in co-cultures with
641 *A. castellanii* trophozoites. This indicates that Sm18 most likely faces manganese and iron
642 restrictions within amoebal phagosomes. *S. maltophilia*'s ability to overcome these limitations
643 through MntH-mediated manganese import may be a key factor in its success as an
644 intracellular pathogen, as found in other bacteria (Anderson et al., 2009; Boyer et al., 2002;
645 Champion et al., 2011; Zaharik et al., 2004), effectively overcoming the host's imposed
646 nutritional immunity (Chandrangsu et al., 2017; Murdoch and Skaar, 2022), an ancient trait of
647 eukaryotic phagocytes conserved from amoebae to macrophages (Yu et al., 2024). Given that
648 *S. maltophilia*, like most Gammaproteobacteria, is a ferrophilic bacterium (see further
649 discussion below), it is not surprising that the Sm18VIM*mntH* mutant did not display
650 significant impairment when grown in defined MOPS medium without Mn (Fig. 7A). This
651 observation suggests that the attenuated replication rate of this mutant in amoebal
652 phagosomes might be due to its limited capacity to contend with reactive oxygen species
653 (ROS), such as superoxide anions and peroxides (Anjem et al., 2009). *S. maltophilia*
654 genomes, including that of Sm18, encode a periplasmic Mn-dependent superoxide dismutase
655 (SOD) and Mn catalase (Crossman et al., 2008). In addition, some enzymes, such as
656 cambialistic SODs (Sendra et al., 2023) or ribonucleotide reductases (Makhlynets et al., 2014;
657 Martin and Imlay, 2011; Wang et al., 2023), can use either Fe or Mn as a co-factor, whereas
658 mismetallation or oxidation via Fenton reactions of iron-containing enzymes in metal-
659 restricted environments in the presence of ROS may be alleviated by using Mn as an
660 alternative co-factor, as described for diverse mononuclear iron enzymes, most notably the
661 key enzyme ribulose-5-phosphate 3-epimerase (Rpe) from the pentose-phosphate pathway
662 (PPP) (Anjem et al., 2009; Imlay, 2014; Sobota and Imlay, 2011). The metallation of Rpe with
663 oxidative stress-resistant Mn^{2+} enables carbon flow through the PPP, producing the NADPH-
664 reducing power required to maintain ROS-countering enzymes, such as glutathione or
665 thioredoxin reductase (Song et al., 2016; Uppalapati and Vazquez-Torres, 2022) in the
666 cytoplasm and diverse periplasmic disulfide isomerases and reductases, probably including
667 the novel pTFP-encoding gene discovered herein.
668 In this study, we analyzed the links between manganese and iron homeostasis systems,
669 focusing on the genes specifically induced by the former under the control of MntR and iron
670 limitation. However, in addition to the MntR miniregulon members, a few other genes were
671 differentially expressed under iron-replete and manganese excess conditions. Of particular
672 relevance was the identification of efflux pumps of the CDF and RND families, as they are
673 know to support intracellular detoxification of zinc and copper during nutritional immunity

(Hood and Skaar, 2012), when iron and manganese concentrations are low, as shown in our integrative model (Fig. 9). Emerging evidence indicates that an imbalanced ratio of transition metals can function as either a direct or indirect regulatory mechanism to mitigate metal toxicity through efflux pumps. The well-studied YiiP (CDF) has been identified as a secondary transporter for manganese export in Salmonella Typhimurium. Notably, its activity is not regulated by Fe or Mn concentrations in the medium, indicating that YiiP may play a role in balancing the levels of other metals (Ouyang et al., 2009). In *Streptococcus pneumoniae*, expression of *czcD*, a zinc CDF efflux pump, is upregulated under Mn(II)-limiting conditions (Ogunniyi et al., 2010). This is consistent with other studies showing that high zinc concentrations can compete with manganese-binding sites on enzymes essential for cellular physiology (Sullivan et al., 2024). In *Bacillus subtilis*, reduced intracellular iron levels heighten cell sensitivity to elevated Co(II) or Mn(II) levels, particularly in strains deficient for export of these metals (Pi et al., 2020). Furthermore, disruption of the Mg(II) efflux system alleviates residual manganese toxicity in an *mntR mntH* mutant, likely by preventing mismetallation through Mg(II) accumulation (Hohle and O'Brian, 2014; Pi et al., 2020). In summary, we hypothesize that under manganese and iron limitation, in addition to uptake systems, Sm18 deploys additional survival mechanisms mediated by transporters that re-establish the balance of transition metal pools by effluxing the most reactive ones, with more favorable free energies (Irving and Williams, 1953; Osman et al., 2019), thereby minimizing mismetallation (Fig. 9). However, the role of the differentially expressed CDF and RND transporters in metal homeostasis needs to be experimentally established in Sm18.

5. Conclusion

This is the first comprehensive analysis of manganese homeostasis in *S. maltophilia.* It revealed a sophisticated network of importers, exporters, and regulatory elements that work coordinately to maintain appropriate intracellular manganese levels. The *S. maltophilia* MntR miniregulon displays intricate connections with Fe and oxidative stress homeostasis systems (Fig. 9). The identification of novel extracytoplasmic components (CQNC-TBDR and pTFP) expands our understanding of bacterial metal homeostasis systems, opening new avenues for future research. The *mntH* gene is required for optimal replication in *Acanthamoeba* trophozoites and in minimal media depleted of Fe and Mn under oxidative stress, although dispensable in complex LB medium. These findings highlight the ferrophilic nature of *S. maltophilia*, advance our knowledge of *S. maltophilia* physiology and adaptation to

intracellular life in phagosomes, contributing to the broader field of bacterial metal homeostasis, potentially opening new strategies to combat infections by this opportunistic, multidrug- and amoeba-resistant pathogen.

CRediT authorship contribution statement

Fulvia Stefany Argueta Zepeda: Writing – original draft, Writing – review & editing, Validation, Methodology, Investigation, Formal analysis, Data curation. **Javier Rivera Campos:** Writing – review & editing, Validation, Methodology. **Julio Valerdi Negreros:** Writing – review & editing, Validation, Methodology. **Christopher Rensing:** Writing – review & editing, Supervision. **Pablo Vinuesa:** Writing – review & editing, Writing – original draft, Supervision, Resources, Project administration, Methodology, Investigation, Funding acquisition, Formal analysis, Conceptualization

Conflict of interest

The authors declare no conflict of interest.

ACKNOWLEDGEMENTS

We thank Alfredo Hernández and Víctor del Moral for their expert technical support and server maintenance at the Centro de Ciencias Genómicas, UNAM. We acknowledge the excellent service provided by personnel at the Unidad de Síntesis y Secuenciación de DNA from Instituto de Biotecnología, UNAM. We thank Dr. Ayari Fuentes from CCG-UNAM for providing access to the multimodal plate reader. We thank Dr. Luis Lozano from the Bioinformatics Unit at CCG-UNAM for his advice and support during the early phase of transcriptome analysis. We thank M.Sc. Laura Cervantes for her laboratory assistance and valuable feedback. We gratefully acknowledge the financial support received from Consejo Nacional de Humanidades Ciencias y Tecnologías (CONAHCyT México, A1-S-11242), Secretaría de Ciencia, Humanidades, Tecnología e Innovación (SECIHTI México CBF-2025-I-1106), and Programa de Apoyo a Proyectos de Investigación e Innovación Tecnológica (PAPIIT), Universidad Nacional Autónoma de México (DGAPA-PAPIIT, UNAM: IN209321 and IN216424) to PV. F. S. A. Z. and J.C.V.N. were recipients of CONAHCyT scholarships 659308 and 745705, respectively.

Appendix A. Supporting information

Supplementary data associated with this article can be found in the online version at doi:10.1016/j.micres.2026 ….

Data availability: The complete genome sequence of *S. maltophilia* Sm18 was deposited in GenBank under accession number CP146374 and the associated genome and transcriptome sequencing reads were deposited under BioProject PRJNA1081934 https://www.ncbi.nlm.nih.gov/bioproject/?term=PRJNA1081934. The RefSeq genome assembly for strain Sm18 is publicly available from NCBI's genome datasets portal at https://www.ncbi.nlm.nih.gov/datasets/genome/GCA_053078355.1/.

The sequence reads generated from the 18 RNAseq samples analyzed in this work were deposited at NCBI's Sequence Read Archive https://www.ncbi.nlm.nih.gov/sra/ under accession numbers SRR36898890 to SRR36898907, as part of BioProject PRJNA1081934 https://www.ncbi.nlm.nih.gov/bioproject/?term=PRJNA1081934.

The hidden Markov models built in this work are freely available from GitHub at: https://github.com/vinuesa/supplementary_materials/tree/main/docs/Argueta-Zepeda_Stenotrophomonas_MntR_miniregulon.

Conflict of interest disclosure statement: None declared.

Ethics statement: None required.

REFERENCES

Abramson, J., Adler, J., Dunger, J., Evans, R., Green, T., Pritzel, A., Ronneberger, O., Willmore, L., Ballard, A.J., Bambrick, J., Bodenstein, S.W., Evans, D.A., Hung, C.-C., O'Neill, M., Reiman, D., Tunyasuvunakool, K., Wu, Z., Žemgulytė, A., Arvaniti, E., Beattie, C., Bertolli, O., Bridgland, A., Cherepanov, A., Congreve, M., Cowen-Rivers, A.I., Cowie, A., Figurnov, M., Fuchs, F.B., Gladman, H., Jain, R., Khan, Y.A., Low, C.M.R., Perlin, K., Potapenko, A., Savy, P., Singh, S., Stecula, A., Thillaisundaram, A., Tong, C., Yakneen, S., Zhong, E.D., Zielinski, M., Žídek, A., Bapst, V., Kohli, P., Jaderberg, M., Hassabis, D., Jumper, J.M., 2024. Accurate structure prediction of biomolecular interactions with AlphaFold 3. Nature 630, 493–500. https://doi.org/10.1038/s41586-024-07487-w

Anderson, E.S., Paulley, J.T., Gaines, J.M., Valderas, M.W., Martin, D.W., Menscher, E., Brown, T.D., Burns, C.S., Roop, R.M., 2009. The Manganese Transporter MntH Is a Critical Virulence Determinant for *Brucella abortus* 2308 in Experimentally Infected Mice. Infect Immun 77, 3466–3474. https://doi.org/10.1128/IAI.00444-09

Andrews, S., 2010. Fastqc: A quality control tool for high throughput sequence data.

Anjem, A., Varghese, S., Imlay, J.A., 2009. Manganese import is a key element of the OxyR response

to hydrogen peroxide in *Escherichia coli*. Molecular Microbiology 72, 844–858. https://doi.org/10.1111/j.1365-2958.2009.06699.x
Anjou, C., Lotoux, A., Morvan, C., Martin-Verstraete, I., 2024. From ubiquity to specificity: The diverse functions of bacterial thioredoxin systems. Environmental Microbiology 26, e16668. https://doi.org/10.1111/1462-2920.16668
Atkinson, H.J., Babbitt, P.C., 2009. An Atlas of the Thioredoxin Fold Class Reveals the Complexity of Function-Enabling Adaptations. PLoS Comput Biol 5, e1000541. https://doi.org/10.1371/journal.pcbi.1000541
Bailey, T.L., Johnson, J., Grant, C.E., Noble, W.S., 2015. The MEME Suite. Nucleic Acids Res 43, W39–W49. https://doi.org/10.1093/nar/gkv416
Blanvillain, S., Meyer, D., Boulanger, A., Lautier, M., Guynet, C., Denancé, N., Vasse, J., Lauber, E., Arlat, M., 2007. Plant Carbohydrate Scavenging through TonB-Dependent Receptors: A Feature Shared by Phytopathogenic and Aquatic Bacteria. PLoS ONE 2, e224. https://doi.org/10.1371/journal.pone.0000224
Blum, M., Andreeva, A., Florentino, L.C., Chuguransky, S.R., Grego, T., Hobbs, E., Pinto, B.L., Orr, A., Paysan-Lafosse, T., Ponamareva, I., Salazar, G.A., Bordin, N., Bork, P., Bridge, A., Colwell, L., Gough, J., Haft, D.H., Letunic, I., Llinares-López, F., Marchler-Bauer, A., Meng-Papaxanthos, L., Mi, H., Natale, D.A., Orengo, C.A., Pandurangan, A.P., Piovesan, D., Rivoire, C., Sigrist, C.J.A., Thanki, N., Thibaud-Nissen, F., Thomas, P.D., Tosatto, S.C.E., Wu, C.H., Bateman, A., 2025. InterPro: the protein sequence classification resource in 2025. Nucleic Acids Research 53, D444–D456. https://doi.org/10.1093/nar/gkae1082
Bolger, A.M., Lohse, M., Usadel, B., 2014. Trimmomatic: a flexible trimmer for Illumina sequence data. Bioinformatics 30, 2114–2120. https://doi.org/10.1093/bioinformatics/btu170
Bosma, E.F., Rau, M.H., van Gijtenbeek, L.A., Siedler, S., 2021. Regulation and distinct physiological roles of manganese in bacteria. FEMS Microbiology Reviews 45, fuab028. https://doi.org/10.1093/femsre/fuab028
Boyer, E., Bergevin, I., Malo, D., Gros, P., Cellier, M.F.M., 2002. Acquisition of Mn(II) in Addition to Fe(II) Is Required for Full Virulence of *Salmonella enterica* Serovar Typhimurium. Infect Immun 70, 6032–6042. https://doi.org/10.1128/IAI.70.11.6032-6042.2002
Brooke, J.S., 2021. Advances in the Microbiology of Stenotrophomonas maltophilia. Clin Microbiol Rev 34, e00030-19. https://doi.org/10.1128/CMR.00030-19
Brooke, J.S., 2012. Stenotrophomonas maltophilia: an Emerging Global Opportunistic Pathogen. Clin Microbiol Rev 25, 2–41. https://doi.org/10.1128/CMR.00019-11
Calvopiña, K., Dulyayangkul, P., Heesom, K.J., Avison, M.B., 2020. TonB-dependent uptake of β-lactam antibiotics in the opportunistic human pathogen Stenotrophomonas maltophilia. Mol Microbiol 113, 492–503. https://doi.org/10.1111/mmi.14434
Čapek, J., Večerek, B., 2023. Why is manganese so valuable to bacterial pathogens? Front. Cell. Infect. Microbiol. 13, 943390. https://doi.org/10.3389/fcimb.2023.943390
Cellier, M., 2001. Polyphyletic origins of bacterial Nramp transporters. Trends in Genetics 17, 365–370. https://doi.org/10.1016/S0168-9525(01)02364-2
Champion, O.L., Karlyshev, A., Cooper, I.A.M., Ford, D.C., Wren, B.W., Duffield, M., Oyston, P.C.F., Titball, R.W., 2011. Yersinia pseudotuberculosis mntH functions in intracellular manganese accumulation, which is essential for virulence and survival in cells expressing functional Nramp1. Microbiology 157, 1115–1122. https://doi.org/10.1099/mic.0.045807-0
Chandrangsu, P., Rensing, C., Helmann, J.D., 2017. Metal homeostasis and resistance in bacteria. Nat Rev Microbiol 15, 338–350. https://doi.org/10.1038/nrmicro.2017.15
Chang, Y.-T., Lin, C.-Y., Chen, Y.-H., Hsueh, P.-R., 2015. Update on infections caused by Stenotrophomonas maltophilia with particular attention to resistance mechanisms and therapeutic options. Front. Microbiol. 6. https://doi.org/10.3389/fmicb.2015.00893
Chauviat, A., Abrouk, D., Brothier, E., Muller, D., Meyer, T., Favre-Bonté, S., 2025. Genomic and phylogenetic re-assessment of the genus Stenotrophomonas: Description of Stenotrophomonas

thermophila sp. nov., and the proposal of Parastenotrophomonas gen. Nov., Pseudostenotrophomonas gen. Nov., Pedostenotrophomonas gen. Nov., and Allostenotrophomonas gen. Nov. Syst Appl Microbiol 48, 126630. https://doi.org/10.1016/j.syapm.2025.126630

Collet, J.-F., Cho, S.-H., Iorga, B.I., Goemans, C.V., 2020. How the assembly and protection of the bacterial cell envelope depend on cysteine residues. Journal of Biological Chemistry 295, 11984–11994. https://doi.org/10.1074/jbc.REV120.011201

Contreras-Moreira, B., Vinuesa, P., 2013. GET_HOMOLOGUES, a Versatile Software Package for Scalable and Robust Microbial Pangenome Analysis. Appl Environ Microbiol 79, 7696–7701. https://doi.org/10.1128/AEM.02411-13

Crossman, L.C., Gould, V.C., Dow, J.M., Vernikos, G.S., Okazaki, A., Sebaihia, M., Saunders, D., Arrowsmith, C., Carver, T., Peters, N., Adlem, E., Kerhornou, A., Lord, A., Murphy, L., Seeger, K., Squares, R., Rutter, S., Quail, M.A., Rajandream, M.-A., Harris, D., Churcher, C., Bentley, S.D., Parkhill, J., Thomson, N.R., Avison, M.B., 2008. The complete genome, comparative and functional analysis of Stenotrophomonas maltophiliareveals an organism heavily shielded by drug resistance determinants. Genome Biol 9, R74. https://doi.org/10.1186/gb-2008-9-4-r74

Denet, E., Vasselon, V., Burdin, B., Nazaret, S., Favre-Bonté, S., 2018. Survival and growth of Stenotrophomonas maltophilia in free-living amoebae (FLA) and bacterial virulence properties. PLoS ONE 13, e0192308. https://doi.org/10.1371/journal.pone.0192308

Dudek, C.-A., Jahn, D., 2022. PRODORIC: state-of-the-art database of prokaryotic gene regulation. Nucleic Acids Research 50, D295–D302. https://doi.org/10.1093/nar/gkab1110

DuMont, A.L., Karaba, S.M., Cianciotto, N.P., 2015. Type II Secretion-Dependent Degradative and Cytotoxic Activities Mediated by Stenotrophomonas maltophilia Serine Proteases StmPr1 and StmPr2. Infect Immun 83, 3825–3837. https://doi.org/10.1128/IAI.00672-15

Eddy, S.R., 2011. Accelerated Profile HMM Searches. PLoS Comput Biol 7, e1002195. https://doi.org/10.1371/journal.pcbi.1002195

Erill, I., 2015. Every Site Counts: Submitting Transcription Factor-Binding Site Information through the CollecTF Portal. J Bacteriol 197, 2454–2457. https://doi.org/10.1128/JB.00031-15

García, C.A., Alcaraz, E.S., Franco, M.A., Passerini De Rossi, B.N., 2015. Iron is a signal for Stenotrophomonas maltophilia biofilm formation, oxidative stress response, OMPs expression, and virulence. Front. Microbiol. 6. https://doi.org/10.3389/fmicb.2015.00926

Hoang, T.T., Karkhoff-Schweizer, R.R., Kutchma, A.J., Schweizer, H.P., 1998. A broad-host-range Flp-FRT recombination system for site-specific excision of chromosomally-located DNA sequences: application for isolation of unmarked Pseudomonas aeruginosa mutants. Gene 212, 77–86. https://doi.org/10.1016/S0378-1119(98)00130-9

Hohle, T.H., O'Brian, M.R., 2014. Magnesium-dependent processes are targets of bacterial manganese toxicity. Molecular Microbiology 93, 736–747. https://doi.org/10.1111/mmi.12687

Hood, M.I., Skaar, E.P., 2012. Nutritional immunity: transition metals at the pathogen–host interface. Nat Rev Microbiol 10, 525–537. https://doi.org/10.1038/nrmicro2836

Hubert, T., Madec, M., Schalk, I.J., 2023. Experimental and computational methods to highlight behavioural variations in TonB-dependent transporter expression in Pseudomonas aeruginosa versus siderophore concentration. Sci Rep 13, 20015. https://doi.org/10.1038/s41598-023-46585-z

Imlay, J.A., 2014. The Mismetallation of Enzymes during Oxidative Stress. Journal of Biological Chemistry 289, 28121–28128. https://doi.org/10.1074/jbc.R114.588814

Irving, H., Williams, R.J.P., 1953. 637. The stability of transition-metal complexes. J. Chem. Soc. 3192–3210. https://doi.org/10.1039/JR9530003192

Juttukonda, L.J., Skaar, E.P., 2015. Manganese homeostasis and utilization in pathogenic bacteria. Molecular Microbiology 97, 216–228. https://doi.org/10.1111/mmi.13034

Kadokura, H., Beckwith, J., 2009. Detecting Folding Intermediates of a Protein as It Passes through the

Bacterial Translocation Channel. Cell 138, 1164–1173. https://doi.org/10.1016/j.cell.2009.07.030
Kalidasan, V., Joseph, N., Kumar, S., Awang Hamat, R., Neela, V.K., 2018. Iron and Virulence in Stenotrophomonas Maltophilia: All We Know So Far. Front. Cell. Infect. Microbiol. 8, 401. https://doi.org/10.3389/fcimb.2018.00401
Kehl-Fie, T.E., Zhang, Y., Moore, J.L., Farrand, A.J., Hood, M.I., Rathi, S., Chazin, W.J., Caprioli, R.M., Skaar, E.P., 2013. MntABC and MntH Contribute to Systemic Staphylococcus aureus Infection by Competing with Calprotectin for Nutrient Manganese. Infect Immun 81, 3395–3405. https://doi.org/10.1128/IAI.00420-13
Kehres, D.G., Zaharik, M.L., Finlay, B.B., Maguire, M.E., 2000. The NRAMP proteins of *Salmonella typhimurium* and *Escherichia coli* are selective manganese transporters involved in the response to reactive oxygen. Molecular Microbiology 36, 1085–1100. https://doi.org/10.1046/j.1365-2958.2000.01922.x
LaBauve, A.E., Wargo, M.J., 2012. Growth and Laboratory Maintenance of *Pseudomonas aeruginosa*. CP Microbiology 25. https://doi.org/10.1002/9780471729259.mc06e01s25
Landeta, C., Boyd, D., Beckwith, J., 2018. Disulfide bond formation in prokaryotes. Nat Microbiol 3, 270–280. https://doi.org/10.1038/s41564-017-0106-2
Langmead, B., Salzberg, S.L., 2012. Fast gapped-read alignment with Bowtie 2. Nat Methods 9, 357–359. https://doi.org/10.1038/nmeth.1923
Liao, C.-H., Lu, H.-F., Yang, C.-W., Yeh, T.-Y., Lin, Y.-T., Yang, T.-C., 2024. HemU and TonB1 contribute to hemin acquisition in Stenotrophomonas maltophilia. Front Cell Infect Microbiol 14, 1380976. https://doi.org/10.3389/fcimb.2024.1380976
Liao, Y., Smyth, G.K., Shi, W., 2019. The R package Rsubread is easier, faster, cheaper and better for alignment and quantification of RNA sequencing reads. Nucleic Acids Research 47, e47–e47. https://doi.org/10.1093/nar/gkz114
Love, M.I., Huber, W., Anders, S., 2014. Moderated estimation of fold change and dispersion for RNA-seq data with DESeq2. Genome Biol 15, 550. https://doi.org/10.1186/s13059-014-0550-8
Makhlynets, O., Boal, A.K., Rhodes, D.V., Kitten, T., Rosenzweig, A.C., Stubbe, J., 2014. Streptococcus sanguinis class Ib ribonucleotide reductase: high activity with both iron and manganese cofactors and structural insights. J Biol Chem 289, 6259–6272. https://doi.org/10.1074/jbc.M113.533554
Martin, J.E., Imlay, J.A., 2011. The alternative aerobic ribonucleotide reductase of Escherichia coli, NrdEF, is a manganese-dependent enzyme that enables cell replication during periods of iron starvation. Mol Microbiol 80, 319–334. https://doi.org/10.1111/j.1365-2958.2011.07593.x
Martin, J.E., Waters, L.S., 2022. Regulation of Bacterial Manganese Homeostasis and Usage During Stress Responses and Pathogenesis. Front. Mol. Biosci. 9, 945724. https://doi.org/10.3389/fmolb.2022.945724
Martin, J.L., 1995. Thioredoxin —a fold for all reasons. Structure 3, 245–250. https://doi.org/10.1016/S0969-2126(01)00154-X
Martínez-García, E., Fraile, S., Algar, E., Aparicio, T., Velázquez, E., Calles, B., Tas, H., Blázquez, B., Martín, B., Prieto, C., Sánchez-Sampedro, L., Nørholm, M.H.H., Volke, D.C., Wirth, N.T., Dvořák, P., Alejaldre, L., Grozinger, L., Crowther, M., Goñi-Moreno, A., Nikel, P.I., Nogales, J., de Lorenzo, V., 2023. SEVA 4.0: an update of the Standard European Vector Architecture database for advanced analysis and programming of bacterial phenotypes. Nucleic Acids Research 51, D1558–D1567. https://doi.org/10.1093/nar/gkac1059
Mavridou, D.A.I., Saridakis, E., Kritsiligkou, P., Mozley, E.C., Ferguson, S.J., Redfield, C., 2014. An Extended Active-site Motif Controls the Reactivity of the Thioredoxin Fold. Journal of Biological Chemistry 289, 8681–8696. https://doi.org/10.1074/jbc.M113.513457
Mikhailovich, V., Heydarov, R., Zimenkov, D., Chebotar, I., 2024. Stenotrophomonas maltophilia virulence: a current view. Front. Microbiol. 15, 1385631. https://doi.org/10.3389/fmicb.2024.1385631

Morey, J.R., McDevitt, C.A., Kehl-Fie, T.E., 2015. Host-imposed manganese starvation of invading pathogens: two routes to the same destination. Biometals 28, 509–519. https://doi.org/10.1007/s10534-015-9850-z

Murdoch, C.C., Skaar, E.P., 2022. Nutritional immunity: the battle for nutrient metals at the host-pathogen interface. Nat Rev Microbiol 20, 657–670. https://doi.org/10.1038/s41579-022-00745-6

Nas, M.Y., White, R.C., DuMont, A.L., Lopez, A.E., Cianciotto, N.P., 2019. Stenotrophomonas maltophilia Encodes a VirB/VirD4 Type IV Secretion System That Modulates Apoptosis in Human Cells and Promotes Competition against Heterologous Bacteria, Including Pseudomonas aeruginosa. Infect Immun 87, e00457-19. https://doi.org/10.1128/IAI.00457-19

Nilewski, S., Varatnitskaya, M., Masuch, T., Kusnezowa, A., Gellert, M., Baumann, A.F., Lupilov, N., Kusnezow, W., Koch, M.-H., Eisenacher, M., Berkmen, M., Lillig, C.H., Leichert, L.I., 2021. Functional metagenomics of the thioredoxin superfamily. J Biol Chem 296, 100247. https://doi.org/10.1074/jbc.RA120.016350

Ochoa-Sánchez, L.E., Vinuesa, P., 2017. Evolutionary Genetic Analysis Uncovers Multiple Species with Distinct Habitat Preferences and Antibiotic Resistance Phenotypes in the Stenotrophomonas maltophilia Complex. Front. Microbiol. 8, 1548. https://doi.org/10.3389/fmicb.2017.01548

Ogunniyi, A.D., Mahdi, L.K., Jennings, M.P., McEwan, A.G., McDevitt, C.A., Van Der Hoek, M.B., Bagley, C.J., Hoffmann, P., Gould, K.A., Paton, J.C., 2010. Central Role of Manganese in Regulation of Stress Responses, Physiology, and Metabolism in *Streptococcus pneumoniae*. J Bacteriol 192, 4489–4497. https://doi.org/10.1128/JB.00064-10

Osman, D., Martini, M.A., Foster, A.W., Chen, J., Scott, A.J.P., Morton, R.J., Steed, J.W., Lurie-Luke, E., Huggins, T.G., Lawrence, A.D., Deery, E., Warren, M.J., Chivers, P.T., Robinson, N.J., 2019. Bacterial sensors define intracellular free energies for correct enzyme metalation. Nat Chem Biol 15, 241–249. https://doi.org/10.1038/s41589-018-0211-4

Ouyang, Z., He, M., Oman, T., Yang, X.F., Norgard, M.V., 2009. A manganese transporter, BB0219 (BmtA), is required for virulence by the Lyme disease spirochete, *Borrelia burgdorferi*. Proc. Natl. Acad. Sci. U.S.A. 106, 3449–3454. https://doi.org/10.1073/pnas.0812999106

Palmer, L.D., Skaar, E.P., 2016. Transition Metals and Virulence in Bacteria. Annu. Rev. Genet. 50, 67–91. https://doi.org/10.1146/annurev-genet-120215-035146

Pan, S.-Y., Shih, Y.-L., Huang, H.-H., Li, L.-H., Lin, Y.-T., Yang, T.-C., 2022. The involvement of PacIRA system of Stenotrophomonas maltophilia in the uptake of Pseudomonas aeruginosa pyochelin and intraspecies competition for iron acquisition. Journal of Microbiology, Immunology and Infection 55, 273–281. https://doi.org/10.1016/j.jmii.2021.03.001

Patzer, S.I., Hantke, K., 2001. Dual Repression by Fe^{2+} -Fur and Mn^{2+} -MntR of the *mntH* Gene, Encoding an NRAMP-Like Mn^{2+} Transporter in *Escherichia coli*. J Bacteriol 183, 4806–4813. https://doi.org/10.1128/JB.183.16.4806-4813.2001

Peracino, B., Buracco, S., Bozzaro, S., 2013. The Nramp (Slc11) proteins regulate development, resistance to pathogenic bacteria and iron homeostasis in Dictyostelium discoideum. J Cell Sci 126, 301–311. https://doi.org/10.1242/jcs.116210

Pi, H., Wendel, B.M., Helmann, J.D., 2020. Dysregulation of Magnesium Transport Protects Bacillus subtilis against Manganese and Cobalt Intoxication. J Bacteriol 202. https://doi.org/10.1128/JB.00711-19

Pompilio, A., Ciavardelli, D., Crocetta, V., Consalvo, A., Zappacosta, R., Di Ilio, C., Di Bonaventura, G., 2014. Stenotrophomonas maltophilia Virulence and Specific Variations in Trace Elements during Acute Lung Infection: Implications in Cystic Fibrosis. PLoS ONE 9, e88769. https://doi.org/10.1371/journal.pone.0088769

Porcheron, G., Garénaux, A., Proulx, J., Sabri, M., Dozois, C.M., 2013. Iron, copper, zinc, and manganese transport and regulation in pathogenic Enterobacteria: correlations between strains, site of infection and the relative importance of the different metal transport systems for

virulence. Front. Cell. Infect. Microbiol. 3. https://doi.org/10.3389/fcimb.2013.00090
Que, Q., Helmann, J.D., 2000. Manganese homeostasis in *Bacillus subtilis* is regulated by MntR, a bifunctional regulator related to the diphtheria toxin repressor family of proteins. Molecular Microbiology 35, 1454–1468. https://doi.org/10.1046/j.1365-2958.2000.01811.x
Rello, J., Kalwaje Eshwara, V., Lagunes, L., Alves, J., Wunderink, R.G., Conway-Morris, A., Rojas, J.N., Alp, E., Zhang, Z., 2019. A global priority list of the TOp TEn resistant Microorganisms (TOTEM) study at intensive care: a prioritization exercise based on multi-criteria decision analysis. Eur J Clin Microbiol Infect Dis 38, 319–323. https://doi.org/10.1007/s10096-018-3428-y
Rivera, J., Valerdi-Negreros, J.C., Vázquez-Enciso, D.M., Argueta-Zepeda, F.-S., Vinuesa, P., 2024. Phylogenomic, structural, and cell biological analyses reveal that *Stenotrophomonas maltophilia* replicates in acidified Rab7A-positive vacuoles of *Acanthamoeba castellanii*. Microbiol Spectr 12, e02988-23. https://doi.org/10.1128/spectrum.02988-23
Ryan, R.P., Monchy, S., Cardinale, M., Taghavi, S., Crossman, L., Avison, M.B., Berg, G., Van Der Lelie, D., Dow, J.M., 2009. The versatility and adaptation of bacteria from the genus Stenotrophomonas. Nat Rev Microbiol 7, 514–525. https://doi.org/10.1038/nrmicro2163
Schauer, K., Rodionov, D.A., De Reuse, H., 2008. New substrates for TonB-dependent transport: do we only see the 'tip of the iceberg'? Trends in Biochemical Sciences 33, 330–338. https://doi.org/10.1016/j.tibs.2008.04.012
Sendra, K.M., Barwinska-Sendra, A., Mackenzie, E.S., Baslé, A., Kehl-Fie, T.E., Waldron, K.J., 2023. An ancient metalloenzyme evolves through metal preference modulation. Nat Ecol Evol 7, 732–744. https://doi.org/10.1038/s41559-023-02012-0
Sengupta, S., Mondal, A., Dutta, D., Parrack, P., 2018. HflX protein protects Escherichia coli from manganese stress. J Biosci 43, 1001–1013. https://doi.org/10.1007/s12038-018-9807-9
Shih, Y.-L., Wu, C.-M., Lu, H.-F., Li, L.-H., Lin, Y.-T., Yang, T.-C., 2022. Involvement of the *hemP-hemA-smlt0796-smlt0797* Operon in Hemin Acquisition by Stenotrophomonas maltophilia. Microbiol Spectr 10, e00321-22. https://doi.org/10.1128/spectrum.00321-22
Shin, H.E., Pan, C., Curran, D.M., Bateman, T.J., Chong, D.H.Y., Ng, D., Shah, M., Moraes, T.F., 2024. Prevalence of Slam-dependent hemophilins in Gram-negative bacteria. J Bacteriol 206, e0002724. https://doi.org/10.1128/jb.00027-24
Si, M., Zhao, C., Burkinshaw, B., Zhang, B., Wei, D., Wang, Y., Dong, T.G., Shen, X., 2017. Manganese scavenging and oxidative stress response mediated by type VI secretion system in *Burkholderia thailandensis*. Proc. Natl. Acad. Sci. U.S.A. 114. https://doi.org/10.1073/pnas.1614902114
Sievers, F., Higgins, D.G., 2018. Clustal Omega for making accurate alignments of many protein sequences. Protein Science 27, 135–145. https://doi.org/10.1002/pro.3290
Silale, A., Van Den Berg, B., 2023. TonB-Dependent Transport Across the Bacterial Outer Membrane. Annu. Rev. Microbiol. 77, 67–88. https://doi.org/10.1146/annurev-micro-032421-111116
Smets, D., Loos, M.S., Karamanou, S., Economou, A., 2019. Protein Transport Across the Bacterial Plasma Membrane by the Sec Pathway. Protein J 38, 262–273. https://doi.org/10.1007/s10930-019-09841-8
Sobota, J.M., Imlay, J.A., 2011. Iron enzyme ribulose-5-phosphate 3-epimerase in Escherichia coli is rapidly damaged by hydrogen peroxide but can be protected by manganese. Proc Natl Acad Sci U S A 108, 5402–5407. https://doi.org/10.1073/pnas.1100410108
Song, F., Zhang, G., Li, H., Ma, L., Yang, N., 2022. Comparative transcriptomic analysis of Stenotrophomonas sp. MNB17 revealed mechanisms of manganese tolerance at different concentrations and the role of histidine biosynthesis in manganese removal. Ecotoxicology and Environmental Safety 244, 114056. https://doi.org/10.1016/j.ecoenv.2022.114056
Song, M., Kim, J.-S., Liu, L., Husain, M., Vázquez-Torres, A., 2016. Antioxidant Defense by Thioredoxin Can Occur Independently of Canonical Thiol-Disulfide Oxidoreductase Enzymatic Activity. Cell Rep 14, 2901–2911. https://doi.org/10.1016/j.celrep.2016.02.066

Sullivan, M.J., Terán, I., Goh, K.G.K., Ulett, G.C., 2024. Resisting death by metal: metabolism and Cu/Zn homeostasis in bacteria. Emerging Topics in Life Sciences 8, 45–56. https://doi.org/10.1042/ETLS20230115

Takahashi, I., Hosomi, K., Nagatake, T., Toubou, H., Yamamoto, D., Hayashi, I., Kurashima, Y., Sato, S., Shibata, N., Goto, Y., Maruyama, F., Nakagawa, I., Kuwae, A., Abe, A., Kunisawa, J., Kiyono, H., 2020. Persistent colonization of non-lymphoid tissue-resident macrophages by *Stenotrophomonas maltophilia*. International Immunology 32, 133–141. https://doi.org/10.1093/intimm/dxz071

Taudte, N., German, N., Zhu, Y.-G., Grass, G., Rensing, C., 2016. Restoration of growth by manganese in a mutant strain of Escherichia coli lacking most known iron and manganese uptake systems. Biometals 29, 433–450. https://doi.org/10.1007/s10534-016-9927-3

The UniProt Consortium, 2017. UniProt: the universal protein knowledgebase. Nucleic Acids Res 45, D158–D169. https://doi.org/10.1093/nar/gkw1099

Uppalapati, S.R., Vazquez-Torres, A., 2022. Manganese Utilization in Salmonella Pathogenesis: Beyond the Canonical Antioxidant Response. Front Cell Dev Biol 10, 924925. https://doi.org/10.3389/fcell.2022.924925

Vinuesa, P., Argueta-Zepeda, F.-S., Valerdi-Negreros, J.C., Vázquez-Enciso, D.M., Osorio-Herrera, M.D., Gutiérrez-Hernández, D., Mendoza-Gómez, K., Rivera, J., 2026. Complete genome sequence of the environmental Stenotrophomonas maltophilia ESTM1D_MKCAZ16_6a (Sm18) strain recovered from sediments of a clean river in Morelos. In revision.

Vinuesa, P., Ochoa-Sánchez, L.E., Contreras-Moreira, B., 2018. GET_PHYLOMARKERS, a Software Package to Select Optimal Orthologous Clusters for Phylogenomics and Inferring Pan-Genome Phylogenies, Used for a Critical Geno-Taxonomic Revision of the Genus Stenotrophomonas. Front. Microbiol. 9, 771. https://doi.org/10.3389/fmicb.2018.00771

Waldron, K.J., Robinson, N.J., 2009. How do bacterial cells ensure that metalloproteins get the correct metal? Nat Rev Microbiol 7, 25–35. https://doi.org/10.1038/nrmicro2057

Wang, N.E., Courcelle, E.J., Coltman, S.M., Spolek, R.L., Courcelle, J., Courcelle, C.T., 2023. Manganese transporters regulate the resumption of replication in hydrogen peroxide-stressed Escherichia coli. Biometals 36, 1361–1376. https://doi.org/10.1007/s10534-023-00523-8

Waters, L.S., 2020. Bacterial manganese sensing and homeostasis. Current Opinion in Chemical Biology 55, 96–102. https://doi.org/10.1016/j.cbpa.2020.01.003

Waters, L.S., Sandoval, M., Storz, G., 2011. The Escherichia coli MntR Miniregulon Includes Genes Encoding a Small Protein and an Efflux Pump Required for Manganese Homeostasis. J Bacteriol 193, 5887–5897. https://doi.org/10.1128/JB.05872-11

Wright, Z., Seymour, M., Paszczak, K., Truttmann, T., Senn, K., Stilp, S., Jansen, N., Gosz, M., Goeden, L., Anantharaman, V., Aravind, L., Waters, L.S., 2024. The small protein MNTS evolved from a signal peptide and acquired a novel function regulating manganese homeostasis in *Escherichia coli*. Molecular Microbiology 121, 152–166. https://doi.org/10.1111/mmi.15206

Wu, C.-M., Li, L.-H., Lin, Y.-L., Wu, C.-J., Lin, Y.-T., Yang, T.-C., 2022. The *sbiTRS* Operon Contributes to Stenobactin-Mediated Iron Utilization in Stenotrophomonas maltophilia. Microbiol Spectr 10, e02673-22. https://doi.org/10.1128/spectrum.02673-22

Xue, K., Song, X., Zhang, W., Zhang, Y., Chen, T., Cao, Z., Hong, F., Zhang, X., 2024. Omics-Based Investigation on Mechanisms Controlling Cellular Internalization of Keratin Monomers during Biodegradation by Stenotrophomonas maltophilia DHHJ. Microb Physiol 34, 170–181. https://doi.org/10.1159/000540072

Yeh, T.-Y., Lu, H.-F., Li, L.-H., Lin, Y.-T., Yang, T.-C., 2025. Contribution of fepAsm, fciABC, sbaA, sbaBCDEF, and feoB to ferri-stenobactin acquisition in Stenotrophomonas maltophilia KJ. BMC Microbiol 25, 91. https://doi.org/10.1186/s12866-025-03792-0

Yu, Y., Li, Y.-P., Ren, K., Hao, X., Fru, E.C., Rønn, R., Rivera, W.L., Becker, K., Feng, R., Yang, J., Rensing, C., 2024. A brief history of metal recruitment in protozoan predation. Trends in Microbiology 32, 465–476. https://doi.org/10.1016/j.tim.2023.11.008

Zaharik, M.L., Cullen, V.L., Fung, A.M., Libby, S.J., Kujat Choy, S.L., Coburn, B., Kehres, D.G., Maguire, M.E., Fang, F.C., Finlay, B.B., 2004. The *Salmonella enterica* Serovar Typhimurium Divalent Cation Transport Systems MntH and SitABCD Are Essential for Virulence in an *Nramp1*^{G169} Murine Typhoid Model. Infect Immun 72, 5522–5525. https://doi.org/10.1128/IAI.72.9.5522-5525.2004

Zeinert, R., Martinez, E., Schmitz, J., Senn, K., Usman, B., Anantharaman, V., Aravind, L., Waters, L.S., 2018. Structure–function analysis of manganese exporter proteins across bacteria. J Biol Chem 293, 5715–5730. https://doi.org/10.1074/jbc.M117.790717

Zhang, T., Wu, H., Ma, C., Yang, Y., Li, H., Yang, Z., Zhou, S., Shi, D., Chen, T., Yang, D., Li, J., Jin, M., 2024. Emergence of colistin-resistant Stenotrophomonas maltophilia with high virulence in natural aquatic environments. Science of The Total Environment 933, 173221. https://doi.org/10.1016/j.scitotenv.2024.173221

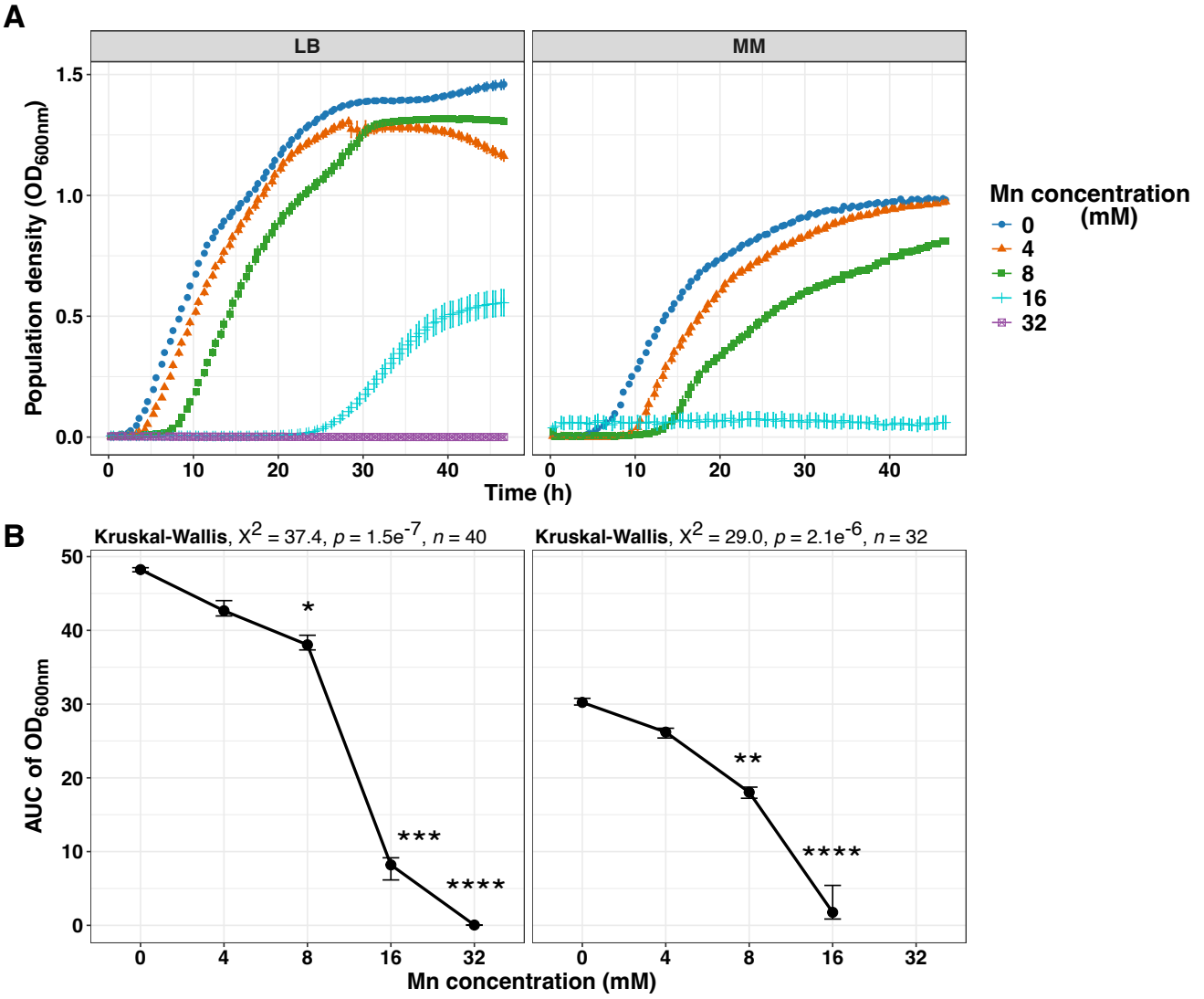

Evaluated contrasts

group1	group2	p.adj	p.adj.signif
0	8	1.101202e−02	*
0	16	1.470991e−04	***
0	32	4.379815e−07	****
4	16	1.101202e−02	*
4	32	1.470991e−04	***
8	32	1.101202e−02	*

group1	group2	p.adj	p.adj.signif
0	8	1.293498e−03	**
0	16	1.864407e−06	****
4	16	1.293498e−03	**

pwc: **Dunn test**; p.adjust: **Benjamini-Hochberg**

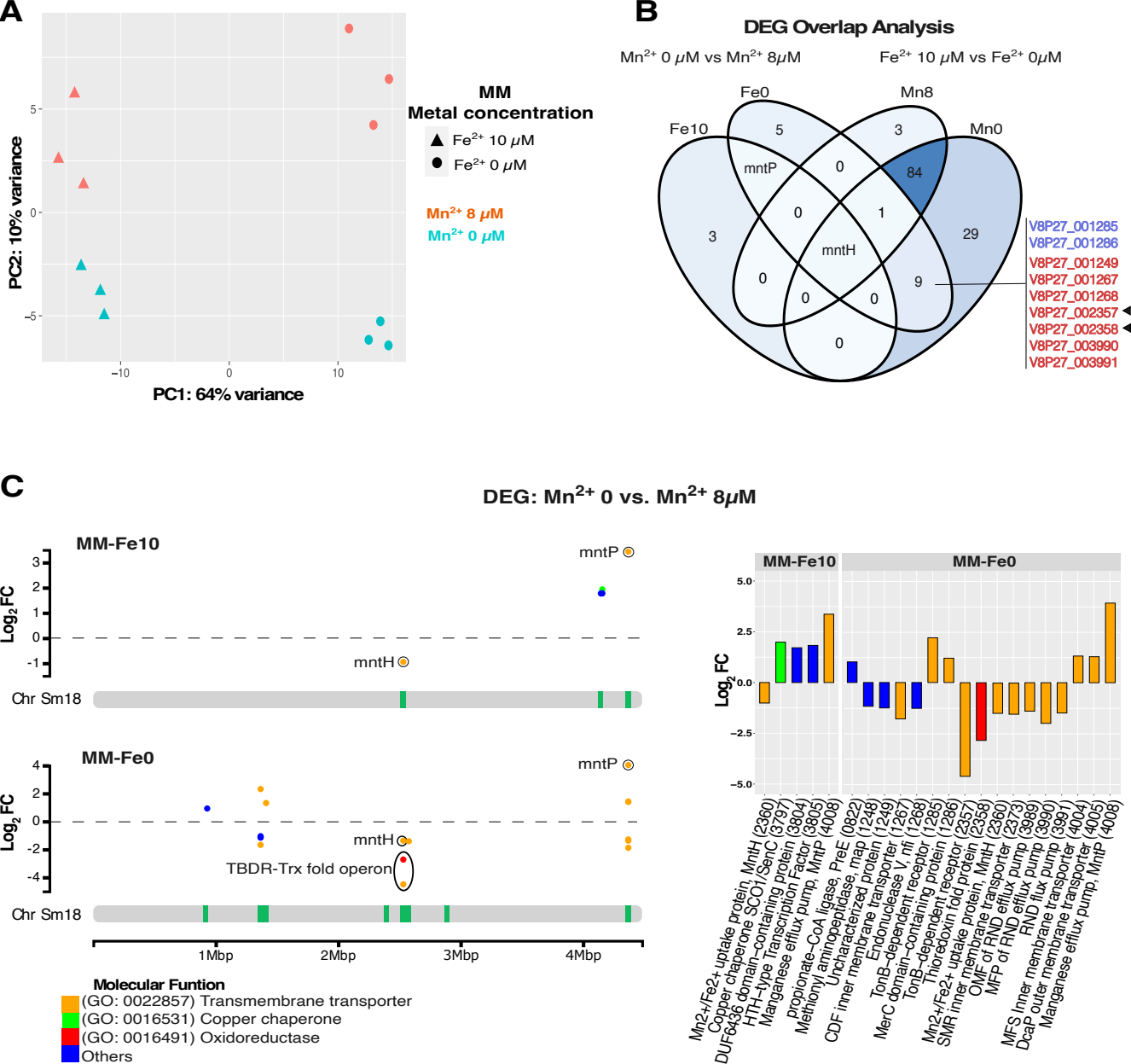
A
PC2: 10% variance
PC1: 64% variance
MM
Metal concentration
Fe2+ 10 μM
Fe2+ 0 μM
Mn2+ 8 μM
Mn2+ 0 μM
B
DEG Overlap Analysis
Mn2+ 0 μM vs Mn2+ 8μM
Fe2+ 10 μM vs Fe2+ 0μM
Fe10
Fe0
Mn8
Mn0
mntP
mntH
V8P27_001285
V8P27_001286
V8P27_001249
V8P27_001267
V8P27_001268
V8P27_002357
V8P27_002358
V8P27_003990
V8P27_003991
C
DEG: Mn2+ 0 vs. Mn2+ 8μM
MM-Fe10
MM-Fe0
Log2FC
mntP
mntH
Chr Sm18
TBDR-Trx fold operon
1Mbp
2Mbp
3Mbp
4Mbp
Molecular Funtion
(GO: 0022857) Transmembrane transporter
(GO: 0016531) Copper chaperone
(GO: 0016491) Oxidoreductase
Others
Mn2+/Fe2+ uptake protein, MntH (2360)
Copper chaperone SCO1/SenC (3797)
DUF6436 domain-containing protein (3804)
HTH-type Transcription Factor (3805)
Manganese efflux pump, MntP (4008)
propionate-CoA ligase, PrpE (0822)
Methionyl aminopeptidase, map (1248)
Uncharacterized protein (1249)
CDF inner membrane transporter (1267)
Endonuclease V, nfi (1268)
TonB-dependent receptor (1285)
TonB-dependent receptor (1286)
Thioredoxin fold protein (2357)
Mn2+/Fe2+ uptake protein, MntH (2358)
SMR inner membrane transporter (2360)
OMF of RND efflux pump (2373)
MFP of RND efflux pump (3989)
RND flux pump (3990)
MFS Inner membrane transporter (3991)
DcaP outer membrane transporter (4004)
Manganese efflux pump, MntP (4005)
(4008)

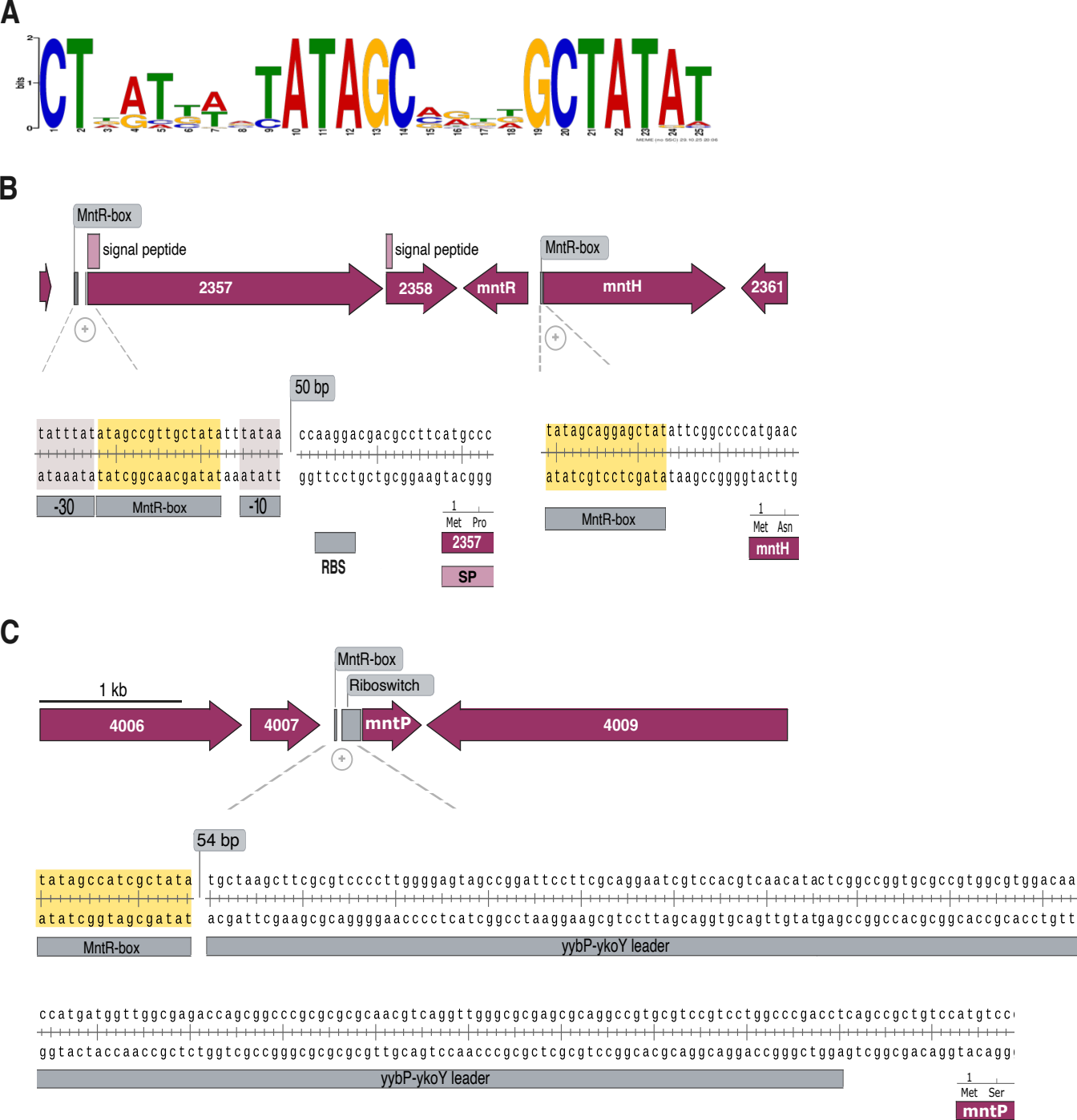
A
bits
B
MntR-box
signal peptide
2357
signal peptide
2358
mntR
MntR-box
mntH
2361
50 bp
tatttatatagccgttgctatatttataa
ataaatatatcggcaacgatataaatatt
ccaaggacgacgccttcatgccc
ggttcctgctgcggaagtacggg
tatagcaggagctatattcggccccatgaac
atatcgtcctcgatataagccggggtacttg
-30
MntR-box
-10
RBS
Met Pro
2357
SP
MntR-box
Met Asn
mntH
C
1 kb
4006
4007
MntR-box
Riboswitch
mntP
4009
54 bp
tatagccatcgctata
atatcggtagcgatat
tgctaagcttcgcgtccccttggggagtagccggattccttcgcaggaatcgtccacgtcaacatactcggccggtgcgccgtggcgtggacaa
acgattcgaagcgcaggggaacccctcatcggcctaaggaagcgtccttagcaggtgcagttgtatgagccggccacgcggcaccgcacctgtt
MntR-box
yybP-ykoY leader
ccatgatggttggcgagaccagcggcccgcgcgcgcaacgtcaggttgggcgcgagcgcaggccgtgcgtccgtcctggcccgacctcagccgctgtccatgtcc
ggtactaccaaccgctctggtcgccgggcgcgcgcgttgcagtccaacccgcgctcgcgtccggcacgcaggcaggaccgggctggagtcggcgacaggtacagg
yybP-ykoY leader
Met Ser
mntP

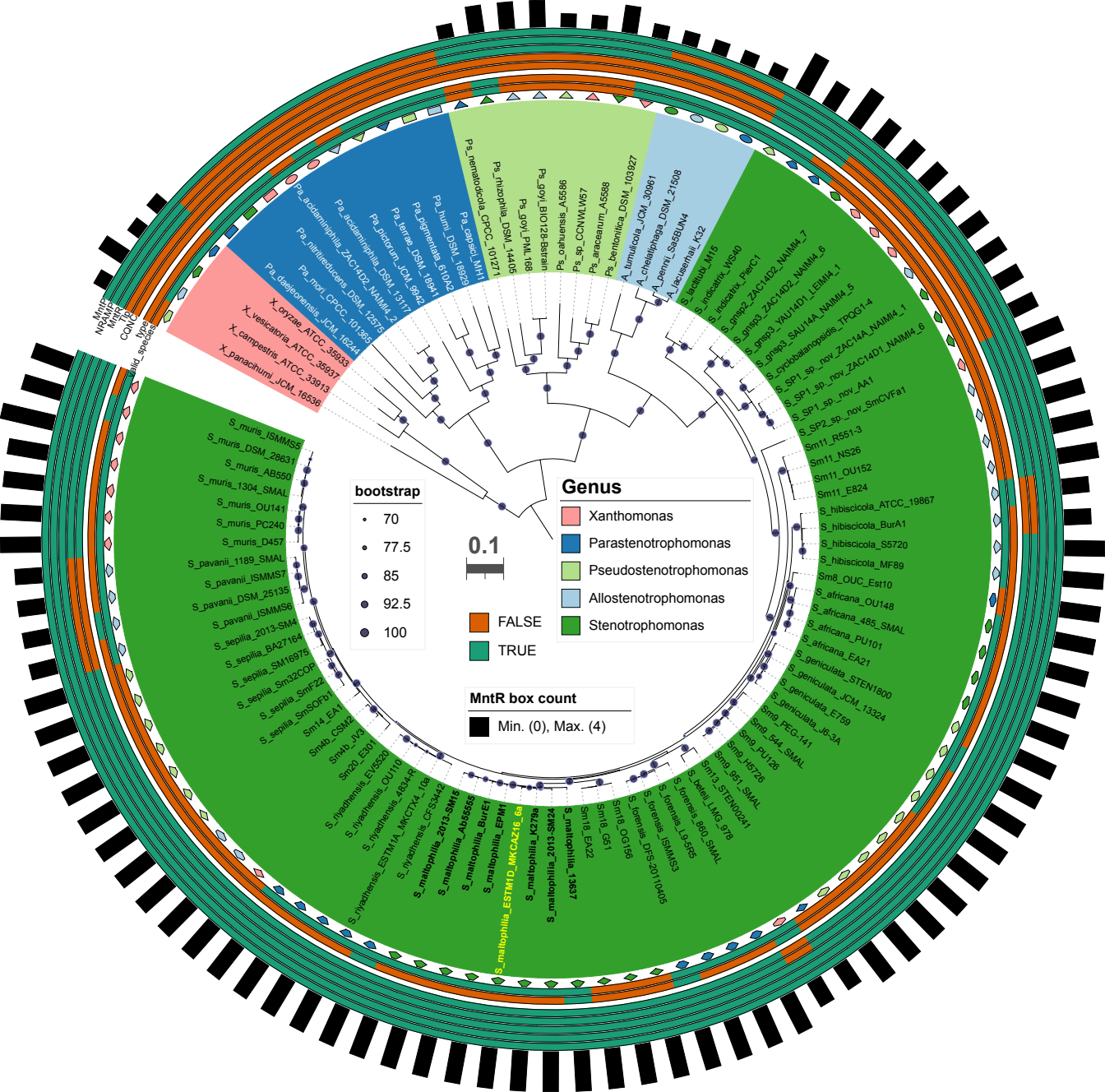
MntR
NRAMP
MntH
CONC
type
valid_species
Pa_nematodicola_CPCC_101271
Pa_rhizophila_DSM_14405
Pa_goyi_PML168
Pa_goyi_CIB128-Serratia
Ps_oahuensis_A5586
Ps_sp._CCNWLW57
Ps_araceanum_A5588
Ps_benitonilica_DSM_103927
A_tumulicola_JCM_30961
A_chelatiphaga_DSM_21508
A_pennyi_Sa5BUN4
A_lacuserhalli_K32
Pa_carpsoli_MH1
Pa_humi_DSM_18929
Pa_pigmentata_610A2
Pa_terrae_DSM_19941
Pa_pictorum_JCM_9942
Pa_acidaminiphila_DSM_13117
Pa_acidaminiphila_ZAC14D2_NAIMI4_2
Pa_mitrifaciens_DSM_12375
Pa_mori_CPCC_101365
Pa_daejeonensis_JCM_16244
X_oryzae_ATCC_35933
X_vesicatoria_ATCC_35937
X_campestris_ATCC_33913
X_panacihumi_JCM_16536
S_lactucae_M15
S_indicatrix_WS40
S_indicatrix_PierC1
S_gnsp2_ZAC14D2_NAIMI4_7
S_gnsp2_ZAC14D2_NAIMI4_6
S_gnsp3_YAU14D1_LEIMI4_1
S_gnsp3_SAU14A_NAIMI4_5
S_cyclobalanopsidis_TPQG1-4
S_SP1_sp._nov_ZAC14A_NAIMI4_1
S_SP1_sp._nov_ZAC14D1_NAIMI4_6
S_SP1_sp._nov_AA1
S_SP2_sp._nov_SmCVFa1
S_SP2_sp._nov_R551-3
Sm11_NS26
Sm11_OU152
Sm11_E824
S_hibiscicola_ATCC_19867
S_hibiscicola_BurA1
S_hibiscicola_S5720
S_hibiscicola_MF89
Sm8_OUC_Est10
S_africana_OU148
S_africana_485_SMAL
S_africana_PU101
S_africana_EA21
S_geniculata_STEN1800
S_geniculata_JCM_13324
S_geniculata_E759
S_geniculata_J6-3A
Sm9_PEG-141
Sm9_544_SMAL
Sm9_PU126
Sm9_H5726
Sm9_951_SMAL
Sm13_STEN00241
S_petalii_LMG_978
S_forensis_860_SMAL
S_forensis_L9-5F5
S_forensis_ISMMS3
S_forensis_DFS_20110405
Sm18_OG156
Sm18_G51
Sm18_EA22
S_maltophilia_13637
S_maltophilia_K279a
S_maltophilia_2013-SM24
S_maltophilia_ESTM1D_MKCAZ16_6a
S_maltophilia_EPM1
S_maltophilia_BurE1
S_maltophilia_Ab555555
S_maltophilia_2013-SM15
S_maltophilia_CFS3442
S_niyadhensis_109
S_niyadhensis_4834-R
S_niyadhensis_OU110
S_niyadhensis_ESTM1A_MKCTX4
S_niyadhensis_EV5520
Sm20_ES01
Sm4b_JK6
Sm14_EA1
Sm4b_CSM2
S_sepilia_SmSOFb1
S_sepilia_SmFZ2
S_sepilia_Sm32COF
S_sepilia_SM16975
S_sepilia_BA27164
S_sepilia_2013-SM4
S_pavanii_DSM_25135
S_pavanii_ISMMS6
S_pavanii_ISMMS7
S_pavanii_1189_SMAL
S_muris_D457
S_muris_PC240
S_muris_OU141
S_muris_1304_SMAL
S_muris_AB550
S_muris_DSM_28631
S_muris_ISMMS5
bootstrap
70
77.5
85
92.5
100
0.1
Genus
Xanthomonas
Parastenotrophomonas
Pseudostenotrophomonas
Allostenotrophomonas
Stenotrophomonas
FALSE
TRUE
MntR box count
Min. (0), Max. (4)

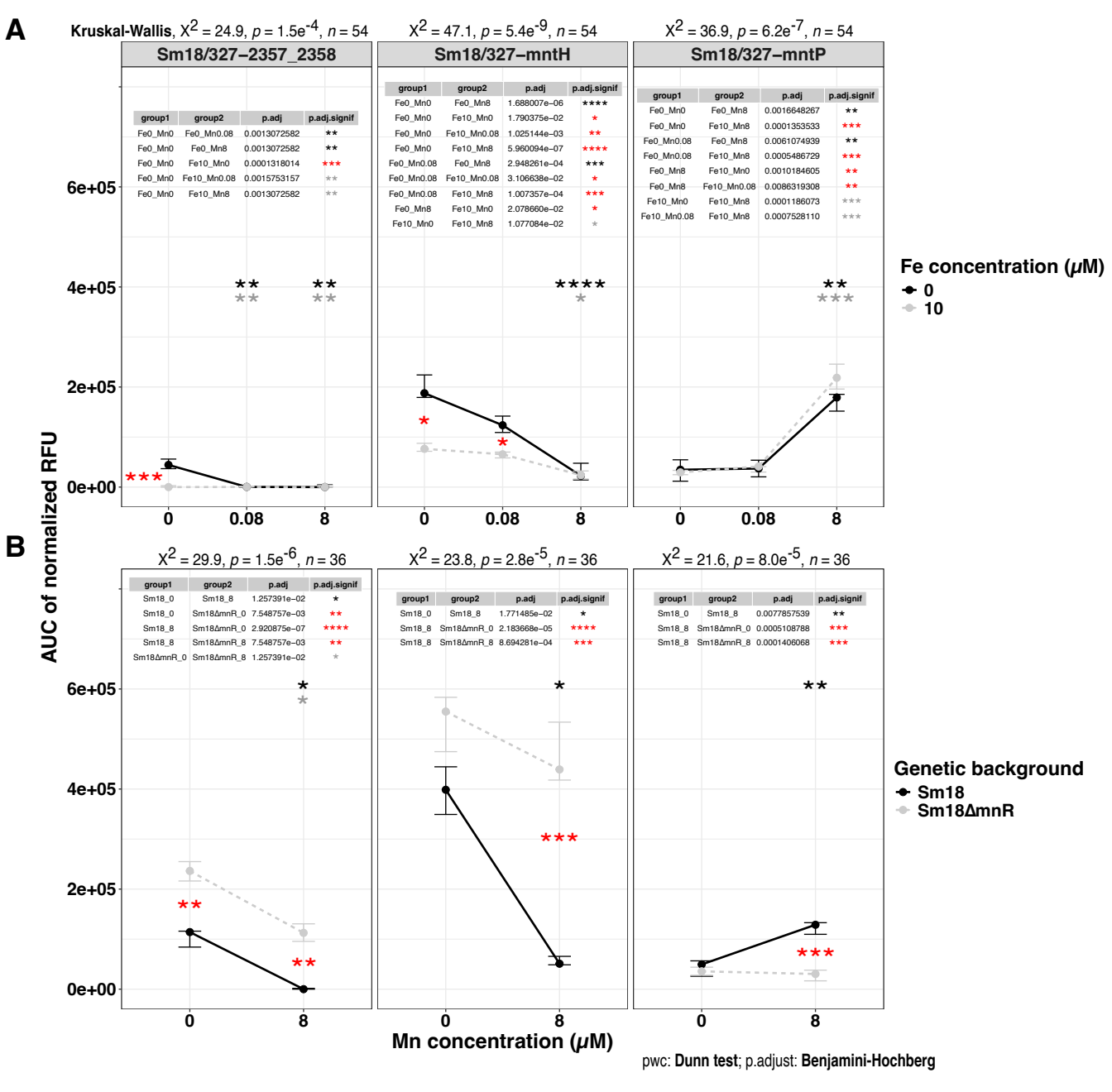
A
Kruskal-Wallis, X^2 = 24.9, p = 1.5e^{-4}, n = 54
X^2 = 47.1, p = 5.4e^{-9}, n = 54
X^2 = 36.9, p = 6.2e^{-7}, n = 54
Sm18/327−2357_2358
Sm18/327−mntH
Sm18/327−mntP
group1 group2 p.adj p.adj.signif
Fe0_Mn0 Fe0_Mn0.08 0.0013072582 **
Fe0_Mn0 Fe0_Mn8 0.0013072582 **
Fe0_Mn0 Fe10_Mn0 0.0001318014 ***
Fe0_Mn0 Fe10_Mn0.08 0.0015753157 **
Fe0_Mn0 Fe10_Mn8 0.0013072582 **
group1 group2 p.adj p.adj.signif
Fe0_Mn0 Fe0_Mn8 1.688007e−06 ****
Fe0_Mn0 Fe10_Mn0 1.790375e−02 *
Fe0_Mn0 Fe10_Mn0.08 1.025144e−03 **
Fe0_Mn0 Fe10_Mn8 5.960094e−07 ****
Fe0_Mn0.08 Fe0_Mn8 2.948261e−04 ***
Fe0_Mn0.08 Fe10_Mn0.08 3.106638e−02 *
Fe0_Mn0.08 Fe10_Mn8 1.007357e−04 ***
Fe0_Mn8 Fe10_Mn0 2.078660e−02 *
Fe10_Mn0 Fe10_Mn8 1.077084e−02 *
group1 group2 p.adj p.adj.signif
Fe0_Mn0 Fe0_Mn8 0.0016648267 **
Fe0_Mn0 Fe10_Mn8 0.0001353533 ***
Fe0_Mn0.08 Fe0_Mn8 0.0061074939 **
Fe0_Mn0.08 Fe10_Mn8 0.0005486729 ***
Fe0_Mn8 Fe10_Mn0 0.0010184605 **
Fe0_Mn8 Fe10_Mn0.08 0.0086319308 **
Fe10_Mn0 Fe10_Mn8 0.0001186073 ***
Fe10_Mn0.08 Fe10_Mn8 0.0007528110 ***
Fe concentration (μM)
0
10
B
X^2 = 29.9, p = 1.5e^{-6}, n = 36
X^2 = 23.8, p = 2.8e^{-5}, n = 36
X^2 = 21.6, p = 8.0e^{-5}, n = 36
group1 group2 p.adj p.adj.signif
Sm18_0 Sm18_8 1.257391e−02 *
Sm18_0 Sm18ΔmnR_0 7.548757e−03 **
Sm18_8 Sm18ΔmnR_0 2.920875e−07 ****
Sm18_8 Sm18ΔmnR_8 7.548757e−03 **
Sm18ΔmnR_0 Sm18ΔmnR_8 1.257391e−02 *
group1 group2 p.adj p.adj.signif
Sm18_0 Sm18_8 1.771485e−02 *
Sm18_8 Sm18ΔmnR_0 2.183668e−05 ****
Sm18_8 Sm18ΔmnR_8 8.694281e−04 ***
group1 group2 p.adj p.adj.signif
Sm18_0 Sm18_8 0.0077857539 **
Sm18_8 Sm18ΔmnR_0 0.0005108788 ***
Sm18_8 Sm18ΔmnR_8 0.0001406068 ***
AUC of normalized RFU
6e+05
4e+05
2e+05
0e+00
0
0.08
8
Mn concentration (μM)
Genetic background
Sm18
Sm18ΔmnR
pwc: Dunn test; p.adjust: Benjamini-Hochberg

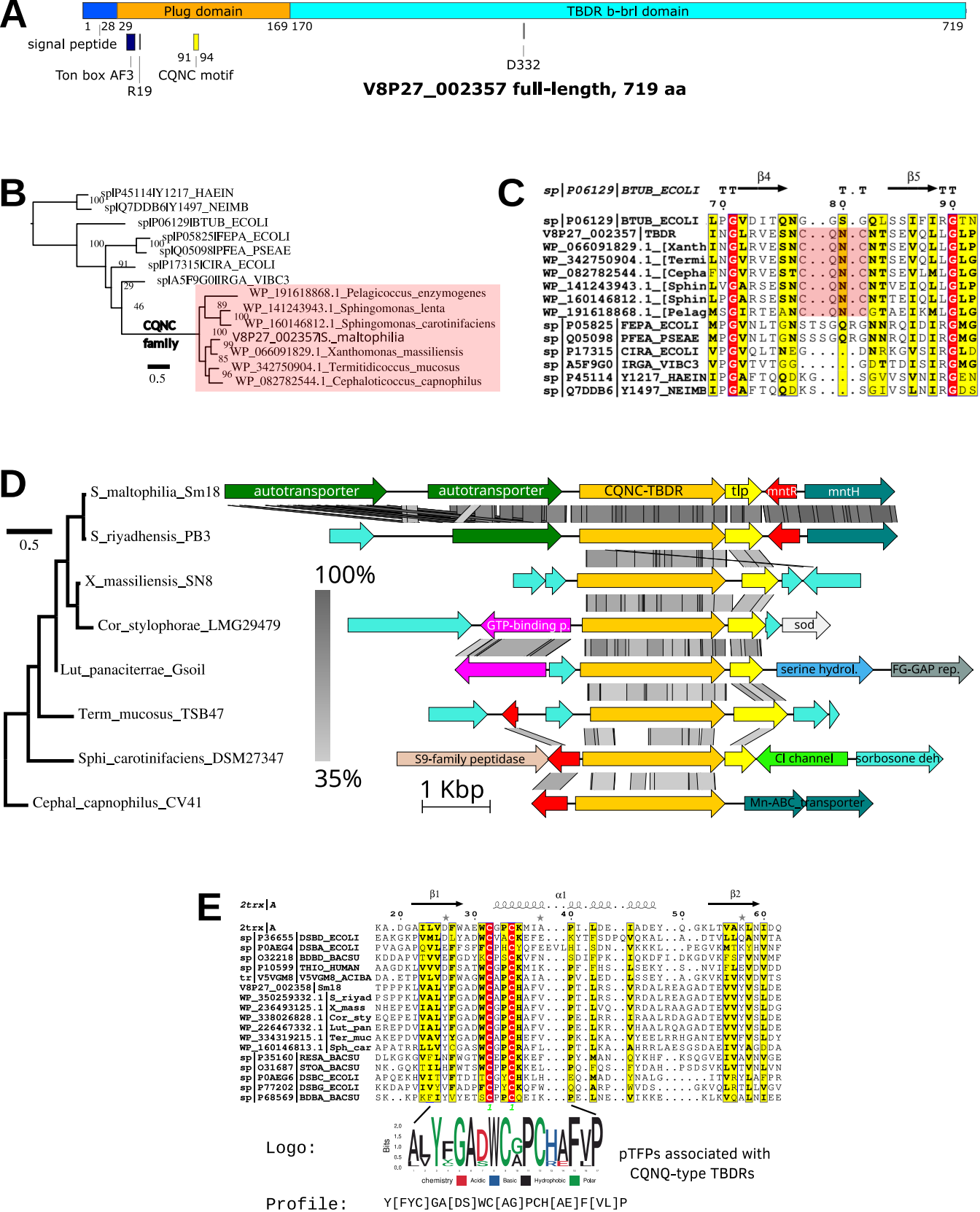
A
Plug domain
TBDR b-brl domain
1 28 29
169 170
719
signal peptide
91 94
Ton box AF3
CQNC motif
R19
D332
V8P27_002357 full-length, 719 aa
B
spIP45114IY1217_HAEIN
spIQ7DDB6IY1497_NEIMB
spIP06129IBTUB_ECOLI
spIP05825IFEPA_ECOLI
spIQ05098IPFEA_PSEAE
spIP17315ICIRA_ECOLI
spIA5F9G0IIRGA_VIBC3
WP_191618868.1_Pelagicoccus_enzymogenes
WP_141243943.1_Sphingomonas_lenta
WP_160146812.1_Sphingomonas_carotinifaciens
V8P27_002357S._maltophilia
WP_066091829.1_Xanthomonas_massiliensis
WP_342750904.1_Termitidicoccus_mucosus
WP_082782544.1_Cephaloticoccus_capnophilus
CQNC
family
0.5
C
sp|P06129|BTUB_ECOLI
β4
β5
sp|P06129|BTUB_ECOLI
V8P27_002357|TBDR
WP_066091829.1_[Xanth
WP_342750904.1_[Termi
WP_082782544.1_[Cepha
WP_141243943.1_[Sphin
WP_160146812.1_[Sphin
WP_191618868.1_[Pelag
sp|P05825|FEPA_ECOLI
sp|Q05098|PFEA_PSEAE
sp|P17315|CIRA_ECOLI
sp|A5F9G0|IRGA_VIBC3
sp|P45114|Y1217_HAEIN
sp|Q7DDB6|Y1497_NEIMB
D
S_maltophilia_Sm18
S_riyadhensis_PB3
X_massiliensis_SN8
Cor_stylophorae_LMG29479
Lut_panaciterrae_Gsoil
Term_mucosus_TSB47
Sphi_carotinifaciens_DSM27347
Cephal_capnophilus_CV41
0.5
autotransporter
autotransporter
CQNC-TBDR
tlp
mntR
mntH
100%
35%
GTP-binding p.
sod
serine hydrol.
FG-GAP rep.
S9-family peptidase
Cl channel
sorbosone deh
1 Kbp
Mn-ABC transporter
E
2trx|A
β1
α1
β2
Logo:
Bits
chemistry
Acidic
Basic
Hydrophobic
Polar
pTFPs associated with
CQNQ-type TBDRs
Profile:
Y[FYC]GA[DS]WC[AG]PCH[AE]F[VL]P

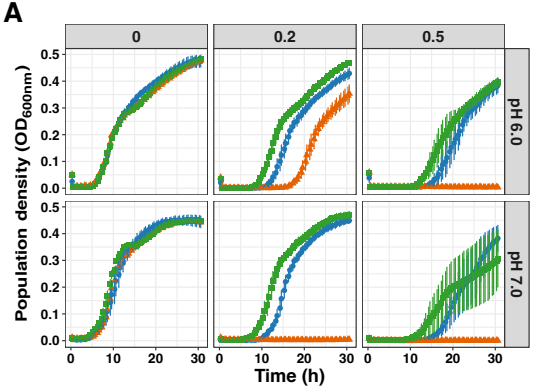
A
0
0.2
0.5
pH 6.0
pH 7.0
Population density (OD600nm)
Time (h)

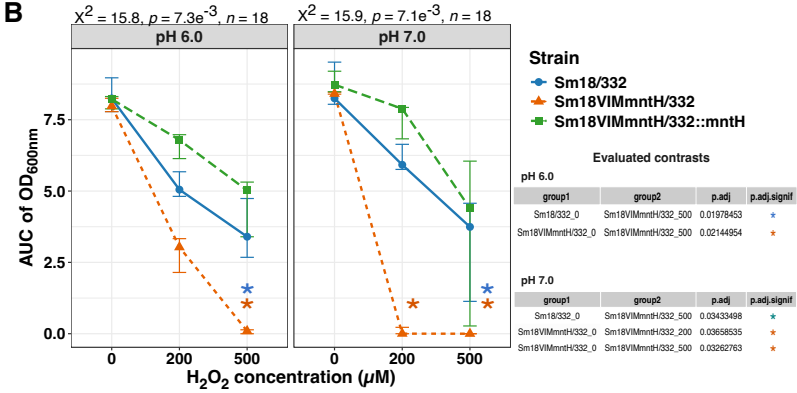
B
X2 = 15.8, p = 7.3e-3, n = 18
X2 = 15.9, p = 7.1e-3, n = 18
pH 6.0
pH 7.0
AUC of OD600nm
H2O2 concentration (μM)
Strain
Sm18/332
Sm18VIMmntH/332
Sm18VIMmntH/332::mntH
Evaluated contrasts
pH 6.0
group1 group2 p.adj p.adj.signif
Sm18/332_0 Sm18VIMmntH/332_500 0.01978453 *
Sm18VIMmntH/332_0 Sm18VIMmntH/332_500 0.02144954 *
pH 7.0
group1 group2 p.adj p.adj.signif
Sm18/332_0 Sm18VIMmntH/332_500 0.03433498 *
Sm18VIMmntH/332_0 Sm18VIMmntH/332_200 0.03658535 *
Sm18VIMmntH/332_0 Sm18VIMmntH/332_500 0.03262763 *

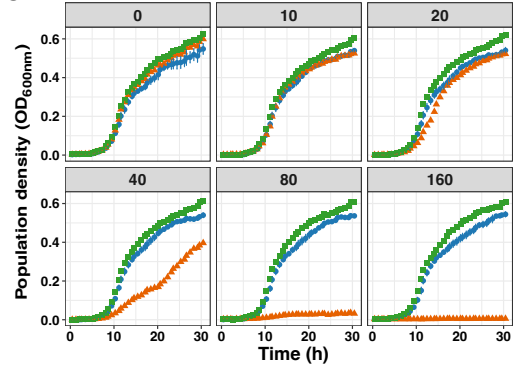
C
0
10
20
40
80
160
Population density (OD600nm)
Time (h)

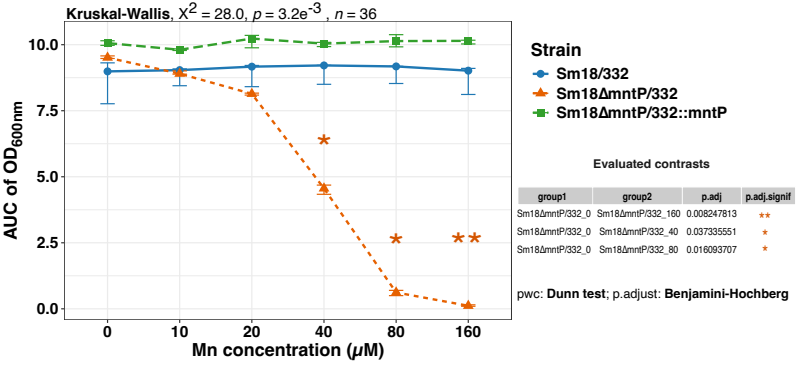
D
Kruskal-Wallis, X2 = 28.0, p = 3.2e-3, n = 36
AUC of OD600nm
Mn concentration (μM)
Strain
Sm18/332
Sm18ΔmntP/332
Sm18ΔmntP/332::mntP
Evaluated contrasts
group1 group2 p.adj p.adj.signif
Sm18ΔmntP/332_0 Sm18ΔmntP/332_160 0.008247813 **
Sm18ΔmntP/332_0 Sm18ΔmntP/332_40 0.037335551 *
Sm18ΔmntP/332_0 Sm18ΔmntP/332_80 0.016093707 *
pwc: Dunn test; p.adjust: Benjamini-Hochberg

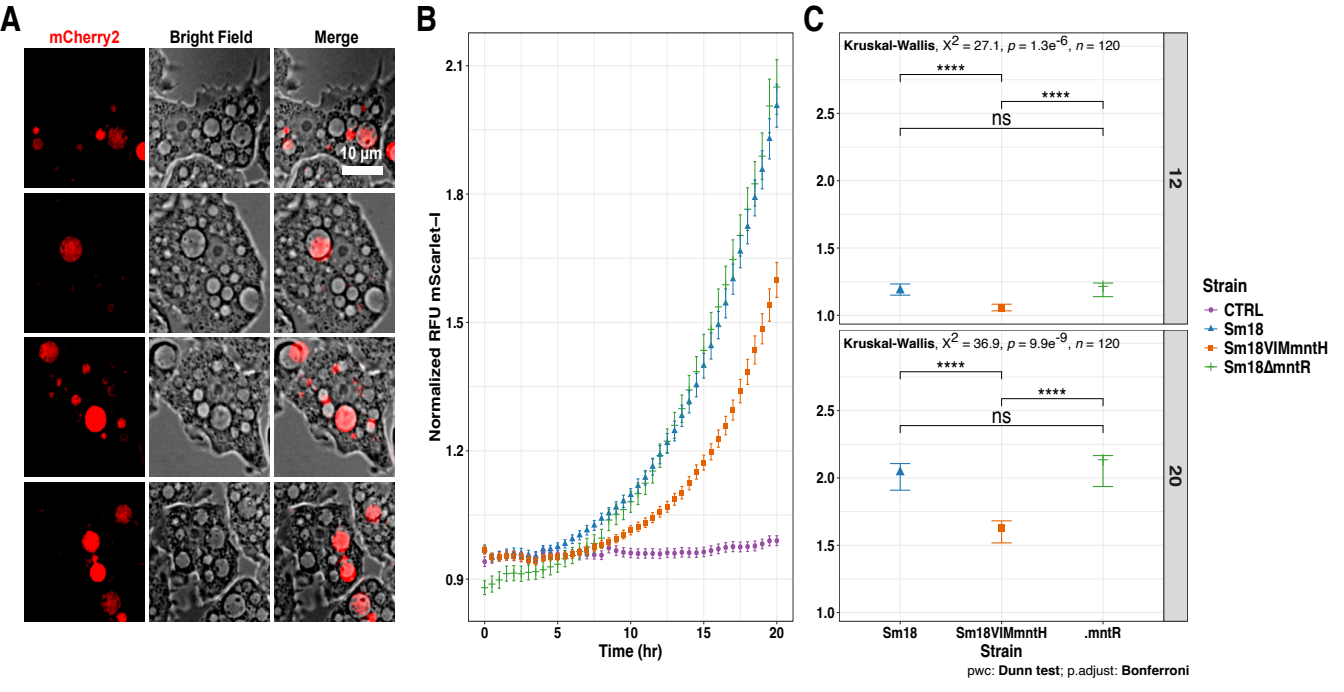
A
mCherry2
Bright Field
Merge
10 µm
B
Normalized RFU mScarlet−I
Time (hr)
C
Kruskal-Wallis, X2 = 27.1, p = 1.3e-6, n = 120
Kruskal-Wallis, X2 = 36.9, p = 9.9e-9, n = 120
****
ns
12
20
Sm18
Sm18VIMmntH
.mntR
Strain
pwc: Dunn test; p.adjust: Bonferroni
Strain
CTRL
Sm18
Sm18VIMmntH
Sm18ΔmntR

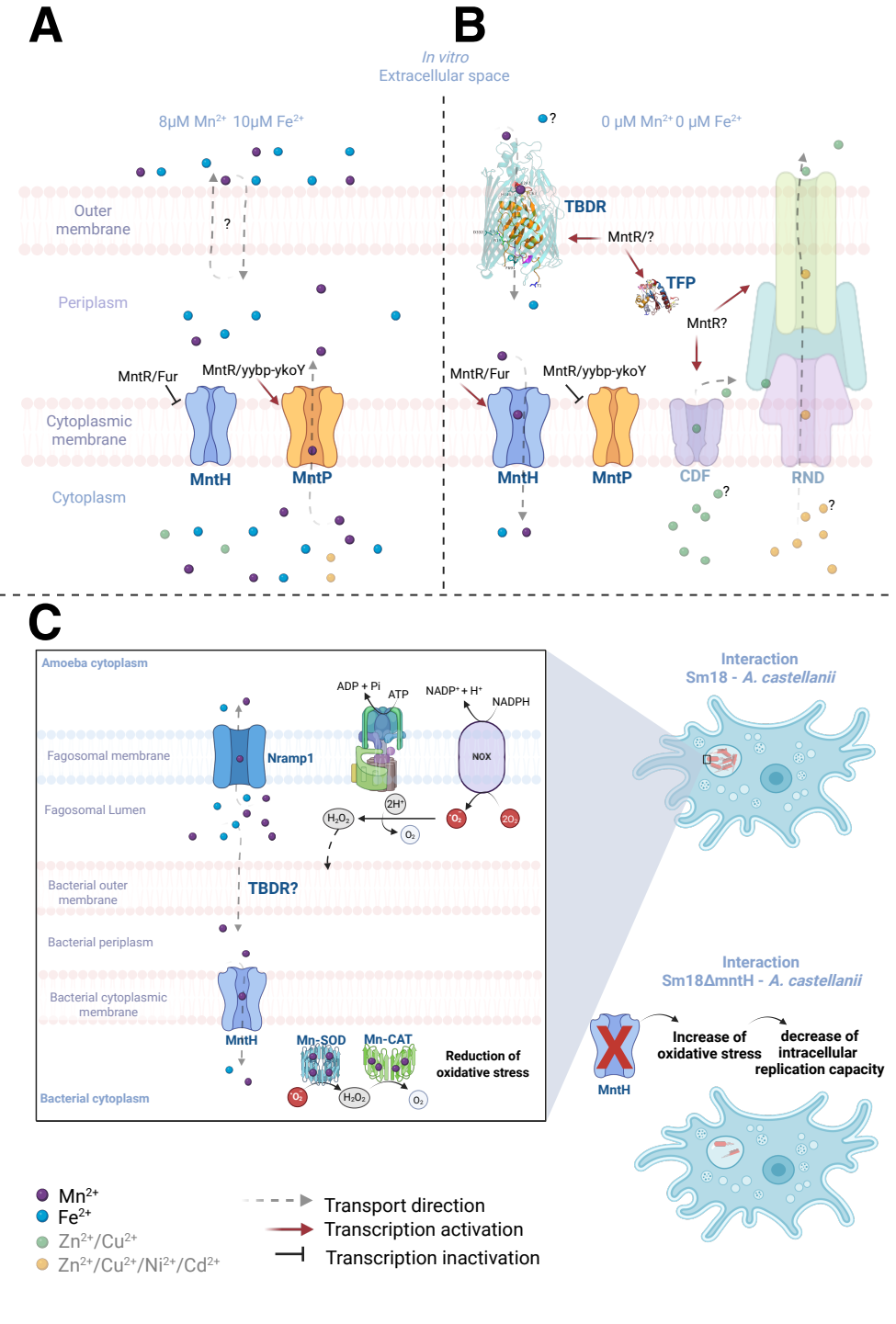
A
8μM Mn2+ 10μM Fe2+
Outer membrane
Periplasm
Cytoplasmic membrane
Cytoplasm
MntR/Fur
MntR/yybp-ykoY
MntH
MntP
B
In vitro
Extracellular space
0 μM Mn2+ 0 μM Fe2+
TBDR
MntR/?
TFP
MntR?
MntR/Fur
MntR/yybp-ykoY
MntH
MntP
CDF
RND
C
Amoeba cytoplasm
Fagosomal membrane
Fagosomal Lumen
Bacterial outer membrane
Bacterial periplasm
Bacterial cytoplasmic membrane
Bacterial cytoplasm
Nramp1
ADP + Pi
ATP
NADP+ + H+
NADPH
NOX
TBDR?
MntH
Mn-SOD
Mn-CAT
Reduction of oxidative stress
Interaction
Sm18 - A. castellanii
Interaction
Sm18ΔmntH - A. castellanii
MntH
Increase of oxidative stress
decrease of intracellular replication capacity
Mn2+
Fe2+
Zn2+/Cu2+
Zn2+/Cu2+/Ni2+/Cd2+
Transport direction
Transcription activation
Transcription inactivation